Precambrian Research 397 (2023) 107197

Contents lists available at ScienceDirect

Precambrian Research

journal homepage: www.elsevier.com/locate/precamres

Age, provenance and tectonic setting of the Tonian–Cryogenian clastic successions in the northwest Bikou terrane, NW Yangtze Block, Central China

Zhidong Gu [a], Xing Jian [b,*], Guixia Liu [a], Xiaotian Shen [b], Hanjing Fu [b], Xiufen Zhai [a], Hua Jiang [a]

[a] Research Institute of Petroleum Exploration and Development (RIPED), PetroChina, Beijing 100083, China
[b] State Key Laboratory of Marine Environmental Science, College of Ocean and Earth Sciences, Xiamen University, Xiamen 361102, China

ARTICLE INFO

Keywords:
Sedimentary provenance
Tectonic setting
Neoproterozoic
Bikou terrane
Yangtze Block

ABSTRACT

Studies on the widely-exposed Neoproterozoic geological records in the Bikou terrane (northwestern Yangtze Block, Central China) have produced different tectonic models (e.g., arc, rift and ridge settings), confusing the relationships between the Bikou and Yangtze blocks in the Neoproterozoic. In addition to the Neoproterozoic Bikou Group igneous rocks and Hengdan Group sedimentary strata which have been well investigated, clastic sedimentary records in the westernmost regions are also crucial for understanding the Neoproterozoic tectonic evolution of the terrane. Here, we target a 3000 m-thick siliciclastic outcrop section along the Bailongjiang River and conduct sedimentological, petrographic, elemental geochemical and zircon U-Pb geochronological analyses to constrain depositional time, sediment provenance and tectonic settings. The outcrop indicates an overall coarsening-upward sedimentary succession, from deep-water sequences to ice-water sequences with dropstone textures. Two volcanic tuffaceous rocks from the basal and middle parts of the succession were dated as 773.2 ± 5.9 Ma and 758.0 ± 8.7 Ma, respectively. The upper parts are characterized by thick, continuous, poorly-sorted glacial diamictites and are conformably overlain by Ediacaran strata. We contend that these diamictites are most likely equivalents to the widespread Cryogenian strata in the Yangtze Block. While provenance analysis results demonstrate felsic bedrock-dominated source terranes with minor mafic contributions, the dropstone gravel components, sandstone petrography and heavy mineral compositions and fine-grained sedimentary rock element concentrations are evidently variable vertically, revealing temporal variations in sediment source-to-sink systems in this region during the late Tonian–Cryogenian. We suggest that the late Tonian deposits were most likely fed by proximal mixed sources with continental arc-related and recycled orogenic terranes, whereas the Cryogenian deposits were dominated by detritus from recycled orogenic terranes. Climate change during the Neoproterozoic glacial-interglacial cycles also played a crucial role in the variable deposit compositions by regulating sediment transport agents and abilities. We favor that the Bikou terrane connected with the Yangtze Block under convergent settings during the early-middle Neoproterozoic and was subsequently under extensional settings. Such findings are a significant step in our understanding of the role of the Yangtze Block in global Neoproterozoic tectonic and climatic frameworks.

1. Introduction

The Neoproterozoic evolution of the Earth, particularly the aspects of tectonics (e.g., the supercontinent cycle and global orogeny), environment and climate change (e.g., the Neoproterozoic Oxygenation Event, ocean redox states and snowball Earth) and biological innovation (e.g., the Ediacarian Biota), are hot topics in Geoscience and have attracted considerable attentions in past decades (e.g., Dalziel, 1997; Hoffman et al., 1998; Och and Shields-Zhou, 2012; Lenton et al., 2014; Merdith et al., 2017). The Yangtze Block in South China documents thick Neoproterozoic sedimentary successions and widespread igneous rocks (ca. 960–720 Ma), which may provide important clues for deciphering Neoproterozoic tectono-sedimentary evolution of the Yangtze Block and its global implications (Wang and Zhou, 2012; Zhao and Cawood, 2012; Dong and Santosh, 2016). The Bikou terrane, located in a wedge-shaped junction region connecting the Yangtze Block, the West Qinling orogen

* Corresponding author.
E-mail address: xjian@xmu.edu.cn (X. Jian).

https://doi.org/10.1016/j.precamres.2023.107197
Received 23 February 2023; Received in revised form 12 September 2023; Accepted 22 September 2023

and the Songpan-Ganzi terrane (Druschke et al., 2006; Hui et al., 2021; Mao et al., 2021), mainly comprises Neoproterozoic geological records. These records are of great significance to understanding early tectonic evolution in Central China and to deciphering the relationships among these terranes during the Neoproterozoic (Yan et al., 2004a; Druschke et al., 2006).

For the past decades since 1940s, considerable investigations have been conducted in the Bikou terrane region regarding its stratigraphy, geochronology, tectonic settings and sedimentary environments (e.g., Pei, 1989; Ding et al., 1998; Kuang et al., 1999; Yan et al., 2003; Lai et al., 2007; Wu et al., 2019; Hui et al., 2021). However, it has long been controversial with respect to the origin and tectonic affinity of the Bikou terrane, in which there are two completely opposite views. One proposition suggests that the Bikou terrane was in an arc (continent/island) setting and developed on the northern margin of the Yangtze Block due to oceanic plate subduction (Pei, 1989; Qin et al., 1994; Yan et al., 2003, 2004a, 2010; Druschke et al., 2006; Li et al., 2006; Dong and Santosh, 2016; Li et al., 2018; Gao et al., 2020a, b; Hui et al., 2020, 2021). The other viewpoint favors that the Neoproterozoic Bikou terrane formed in a rift setting due to continental breakup (Ding et al., 1998; Kuang et al., 1999; Xia et al., 1999; Xu et al., 2002; Li et al., 2007; Wu et al., 2019). In addition to the two main views, some other viewpoints and tectonic models have also been put forward, such as considering the terrane as a Meso-Neoproterozoic microcontinent (e.g., Meng and Zhang, 2000; Zhang et al., 1996), mid-ocean ridge settings (Lai et al., 2007), presence of widespread continental flood basalts (Wang et al., 2008), or back-arc basin settings (Hui et al., 2021). These controversies and distinct models have hindered better understanding of the early evolution of the Bikou terrane and its role in assembling process of the surrounding blocks. Although substantial attentions have been drawn, previous studies mainly focused on igneous rocks of the Bikou Group in the southeastern Bikou terrane and on clastic rocks of the Hengdan Group in the northwest area. Investigations on the Neoproterozoic clastic sedimentary successions in the westernmost Bikou terrane, especially their sedimentary sources, transport processes and depositional mechanisms, are expected to provide substantial clues to unraveling those controversies.

In this study, we target the 3000 m-thick Neoproterozoic siliciclastic strata exposed along the Bailongjiang River in the northwestern Bikou terrane and conduct an integrated study involving field-based sedimentology, petrography, zircon U-Pb geochronology and elemental geochemistry. The purposes are 1) to constrain depositional periods of the well-exposed clastic successions, 2) to determine sedimentary provenance and depositional environments and 3) to reconstruct the tectono-sedimentary evolution history of the Neoproterozoic Bikou terrane. This study does not only provide insight on the tectonics of the northwest Yangtze Block, but would also shed light on global Neoproterozoic tectonics and climate.

2. Geological setting

2.1. The Bikou terrane and the surrounding tectonic domains

The South China Craton consists of the Yangtze Block in the northwest and the Cathaysia Block in the southeast. These two blocks were assembled together along the Jiangnan orogen at ca. 820 Ma during the early Neoproterozoic (Fig. 1A) (Zhao and Cawood, 2012; Cawood et al., 2013; Domeier, 2018). The northwest portion of the present-day Yangtze Block contains the Sichuan Basin, the Micangshan-Hannan terrane, the Longmenshan fold-thrust belt, and the Bikou terrane, which are separated with the West Qinling orogen by the Mianlue suture. The West Qinling orogen is bounded by the Wushan-Tianshui suture to the north and Mianlue suture to the south (Pei et al., 2004) (Fig. 1B). The Qinling orogenic belt is regarded as the boundary between the North and South China Cratons (Meng and Zhang, 1999; Druschke et al., 2006; Dong et al., 2015; Hui et al., 2020) (Fig. 1B).

The Bikou terrane lies across the border of Shaanxi, Gansu, and Sichuan provinces geographically in Central China (Pei, 1989), and connects the Longmenshan fold-thrust belt, the West Qinling orogen, and the Songpan-Ganzi terrane geologically (Yan et al., 2004a). It is bounded with the Longmenshan fold-thrust belt by the Pingwu-Qingchuan fault to the southeast, bounded with the West Qinling orogen by the Mianlue suture to the north, and contacts with the Songpan-Ganzi terrane by the Huyaguan fault to the southwest (Hui et al., 2021) (Fig. 2).

2.2. Geological records in the Bikou terrane

The Neoarchean Yudongzhi Group is restrictedly located in the northeast margin of the terrane and is considered as the oldest rock unit in this region (Hui et al., 2017, 2019). It mainly comprises granitoid gneisses (ca. 2.82–2.45 Ga), amphibolites (ca. 2.70 Ga), and some metasedimentary rocks (Xiao et al., 2007; Yan et al., 2018; Hui et al., 2017, 2019) (Fig. 2A). The most widespread strata exposure in the Bikou terrane includes the Bikou Group to the southeast and the Hengdan Group to the northwest by the Fengxiangyuan-Tongqianba fault (Yan et al., 2004a; Wu et al., 2019; Fig. 2). These strata unconformably overlie the Yudongzhi Group. The Bikou Group is composed mainly of volcanic successions including the lower mafic to intermediate rocks and the upper felsic rocks, with minor marine and volcaniclastic sedimentary interbeds (Druschke et al., 2006; Xiao et al., 2007). The Hengdan Group consists mainly of a thick (ca. 10–15 km) succession of coarsening-upward, deep marine, pelagic- to turbidite-dominated volcaniclastic deposits (Yan et al., 2004a; Druschke et al., 2006). Both of the Bikou and Hengdan Groups underwent strong deformation and low greenschist facies metamorphism (Yan et al., 2003, 2004a; Druschke et al., 2006; Hui et al., 2021). Age of the Bikou Group volcanic rocks were well constrained from ca. 846 to 776 Ma based on SHRIMP U-Pb dating (Yan et al., 2003, 2004a; Wang et al., 2008), while detrital zircon dating from clastic rocks of the Hengdan Group yields ages from ca. 850 to 700 Ma with a peak near 770 Ma (Druschke et al., 2006), ages ranging from ca. 741 to 717 Ma (Gao et al., 2020b), or ages <720 Ma (Hui et al., 2020), revealing the maximum depositional ages of the Tonian period.

Several gabbroic-granitoid plutons with the Neoproterozoic crystalline ages are northeasterly distributed within the southeastern domain of the Bikou terrane (Xiao et al., 2007; Hui et al., 2021), including the Dongjiahe gabbro (839.2 ± 8.2 Ma, Lai et al., 2007), the Pingtoushan diorite (884 ± 5.5 Ma, Xiao et al., 2007), the Guankouya diorite (884 ± 13 Ma, Xiao et al., 2007), the Liujiaping gabbro (877 ± 13 Ma, Xiao et al., 2007), the Huayangou gabbro-diorite (882 ± 4 Ma, Hui et al., 2021), and the Linhouba gabbro (882 ± 5 Ma, Hui et al., 2021) (Fig. 2A). A series of small-scale mafic dike swarms intruding the Bikou terrane have been dated as ca. 689 and 660–652 Ma (Yan et al., 2004a).

The westernmost Neoproterozoic sedimentary exposure in the Bikou terrane is named as Guanjiagou Formation in most literatures and in previous Chinese geological documents (e.g., Su et al., 2003; Yan et al., 2004b; Lu et al., 2005, 2006; Wang et al., 2010). It unconformably overlies the Hengdan Group, representing Neoproterozoic glacial deposits-dominated sedimentary successions (Druschke et al., 2006; Mao et al., 2021). The Guanjiagou Formation is overlain by the Ediacaran-Lower Cambrian slope-basin facies carbonate rocks, siliciclastic rocks and cherts. These Ediacaran-Lower Cambrian strata are generally unconformably overlain by Devonian strata. The absence of most lower Paleozoic strata might be a result of multiphase tectonic activities.

3. Samples and methods

3.1. Samples

The Neoproterozoic succession at the Gaofengcun section comprises various sedimentary rocks (Fig. 3). To better constrain the depositional period, volcanic tuffaceous rock (samples 2021HZD-02 and 2021GFC-

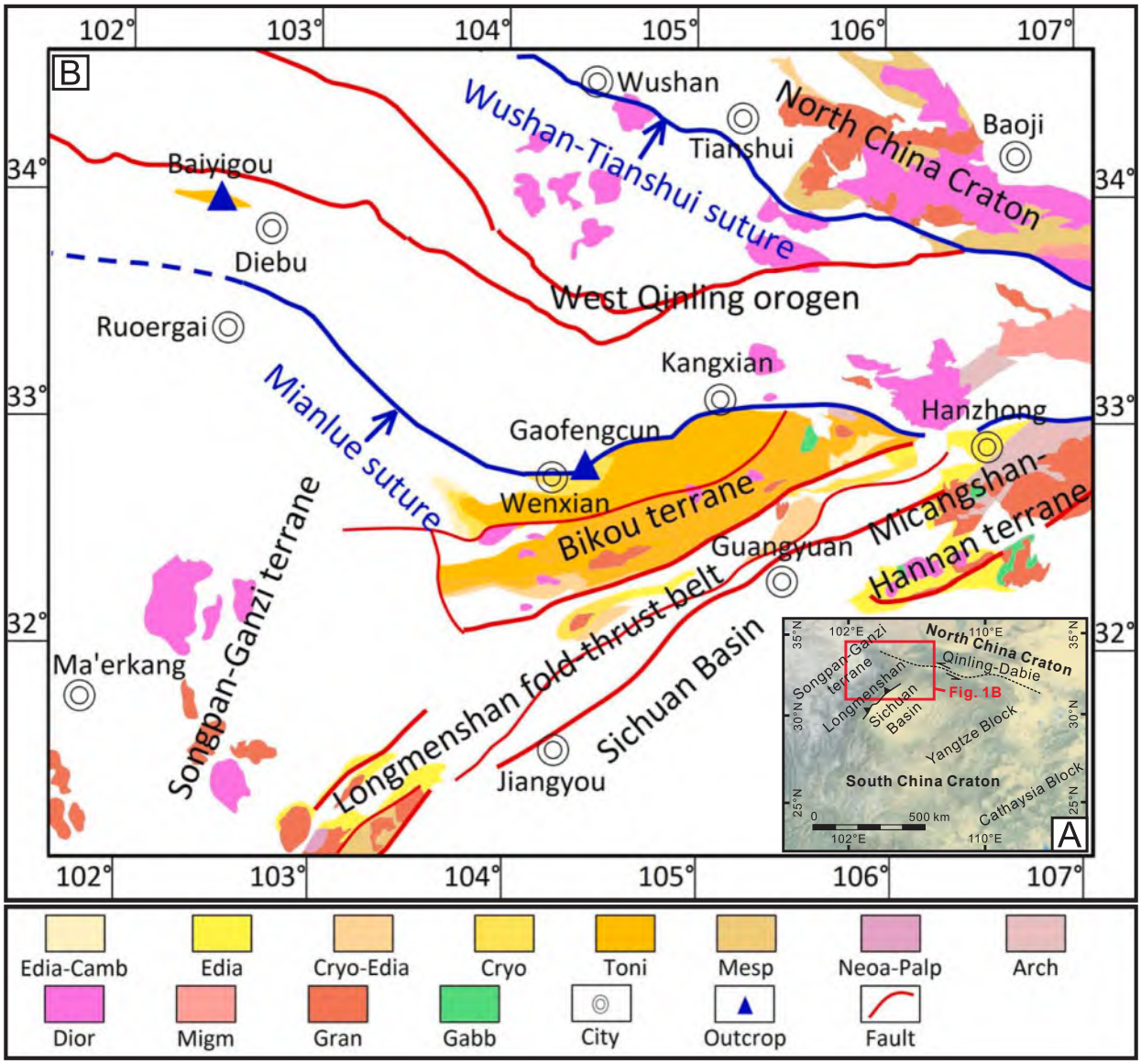

Fig. 1. Regional maps for the study area. (A) a map showing major tectonic domains (modified from Jian et al. (2019a)); (B) a simplified geological map of the Bikou terrane and the surrounding regions (modified from Gu et al. (2023)). Edia-Camb: Ediacaran-Cambrian; Edia: Ediacaran; Cryo-Edia: Cryogenian-Ediacaran; Cryo: Cryogenian; Toni: Tonian; Mesp: Mesoproterozoic; Neoa-Palp: Neoarchean-Paleoproterozoic; Arch: Archean; Dior: diorite; Migm: migmatite; Gran: granite; Gabb: gabbro.

25), granite gravel in glacial diamictite (sample 2021GFC-12) and sandstone (sample 21GFC-32) samples were collected from the investigated outcrop. The former three samples were analyzed for SHRIMP U-Pb zircon dating, and the last detrital sample was analyzed for LA-ICP-MS U-Pb zircon dating. Furthermore, forty-six sandstones (including greywacke) samples were selected and polished into standard thin sections for detrital framework petrography analysis. Twenty sandstone samples were treated for heavy mineral analysis. Forty-nine fine-grained sedimentary rock samples (mainly including mudstones, silty mudstones and tuffaceous rocks) were selected for collecting major, trace and rare earth element geochemical data.

3.2. Methods

3.2.1. Zircon U-Pb geochronology

Zircon grains were separated using conventional density and magnetic techniques and were then carefully hand-picked under a binocular microscope. The separated zircon grains were mounted in epoxy resin and polished to half section to expose their internal structure. All the mounted zircon grains were photographed under reflected and transmitted light, followed by cathode luminescence imaging for targeting domains within grains for isotopic analysis (Gu et al., 2023).

Zircon U-Pb isotopic analyses of samples 2021HZD-02, 2021GFC-25 and 2021GFC-12 were performed on a SHRIMP || at the Beijing SHRIMP Center, the Institute of Geology, Chinese Academy of Geological Sciences, using the standard operating conditions (5-scan duty cycle, 4.5nA and 10 kV primary O^{-2} beam, mass resolution ca. 5000). The method of SHRIMP dating was given in detail by Yan et al. (2003) and Druschke et al. (2006). Zircon standard SL13 (U = 238 ppm, reference age of 572 Ma) was used for calibrating the U contents, and zircon standard TEMORA ($^{206}Pb/^{238}U = 0.0668$, reference age of 417 Ma) was used for calibrating the $^{206}Pb/^{238}U$ ratios. Measured compositions were corrected for common Pb using measured ^{204}Pb. The SQUID and ISOPLOT/Ex software packages were used for data reduction (Wang et al., 2008). Weighted mean $^{206}Pb/^{238}U$ ages with 1σ error are at the 95% confidence level. The zircon U-Pb isotopic analysis of the sample 21GFC-32 was

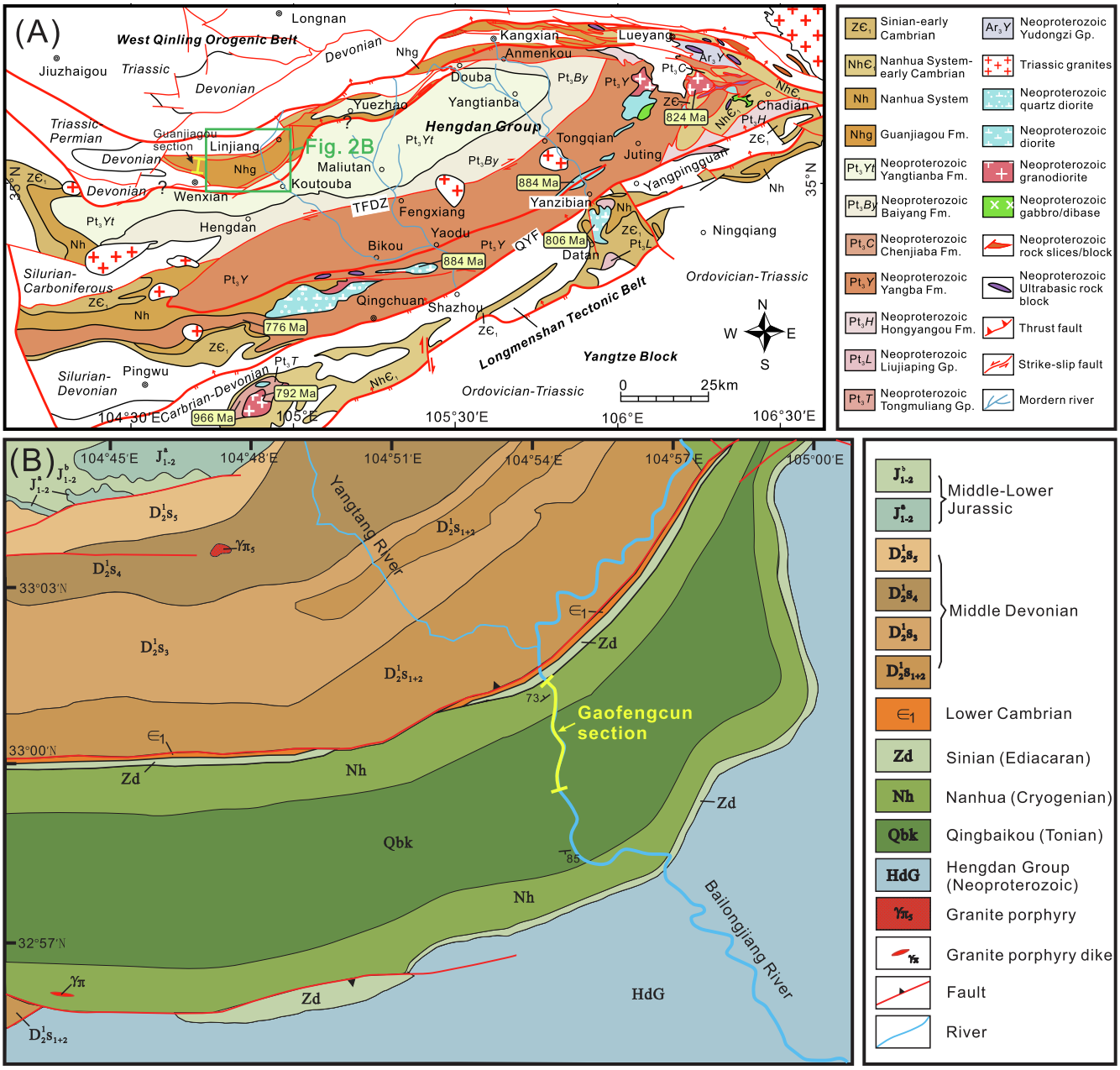

Fig. 2. (A) A geological map of the Bikou terrane (modified from Gao et al. (2020a)). Representative granitoid rock ages (zircon U-Pb dating) are from Hui et al. (2021). (B) A geological map (1:200000) of the study area and the location of the Gaofengcun section. The investigated section is along with the Bailongjiang River and located at north limb of an anticline in the Bikou terrane.

conducted by a LA-ICP-MS at the Mineral Laser Microprobe Analysis Laboratory (Milma Lab), China University of Geosciences, Beijing (CUGB), China. The detailed analytical methods have been described by Zhang et al. (2019). The common-Pb correction followed the method of Anderson (2002). Analysis results are presented with 2σ error and in concordia diagrams. $^{207}Pb/^{206}Pb$ age is used as a more precise result for zircons older than 1000 Ma, while $^{206}Pb/^{238}U$ age is taken for zircons younger than 1000 Ma (Gu et al., 2023).

3.2.2. Petrography

The sedimentary rock thin sections were observed and investigated under a polarizing microscope. Major framework grains in the sandstones, including quartz, plagioclase, K-feldspar and various lithic fragments, were identified. Texture of the samples was also concerned. Modal analysis of the selected samples was performed using the Gazzi-Dickinson method (Dickinson, 1985) and more than 400 points were counted for each thin section (Jian et al., 2023).

3.2.3. Heavy mineral analysis

Heavy mineral analysis was carried out by following procedures described by Gu et al. (2023) and Jian et al. (2023). The sandstone samples were first simply broken in a crushing tank. Then, 63–250 μm fractions were separated with sieves. These 63–250 μm fraction grains were soaked in 1 N acetic acid for 24 hrs under 60 degrees Celsius to remove carbonate minerals. Heavy minerals were separated from the carbonate-free 63–250 μm fractions by heavy liquid tribromomethane (2.89 g/cm^3). The separated grains were then washed and mounted on glass slides with Canada balsam. About 200 transparent heavy mineral grains were identified and point-counted at suitable regular spacing under a polarizing microscope. Morphological features were also

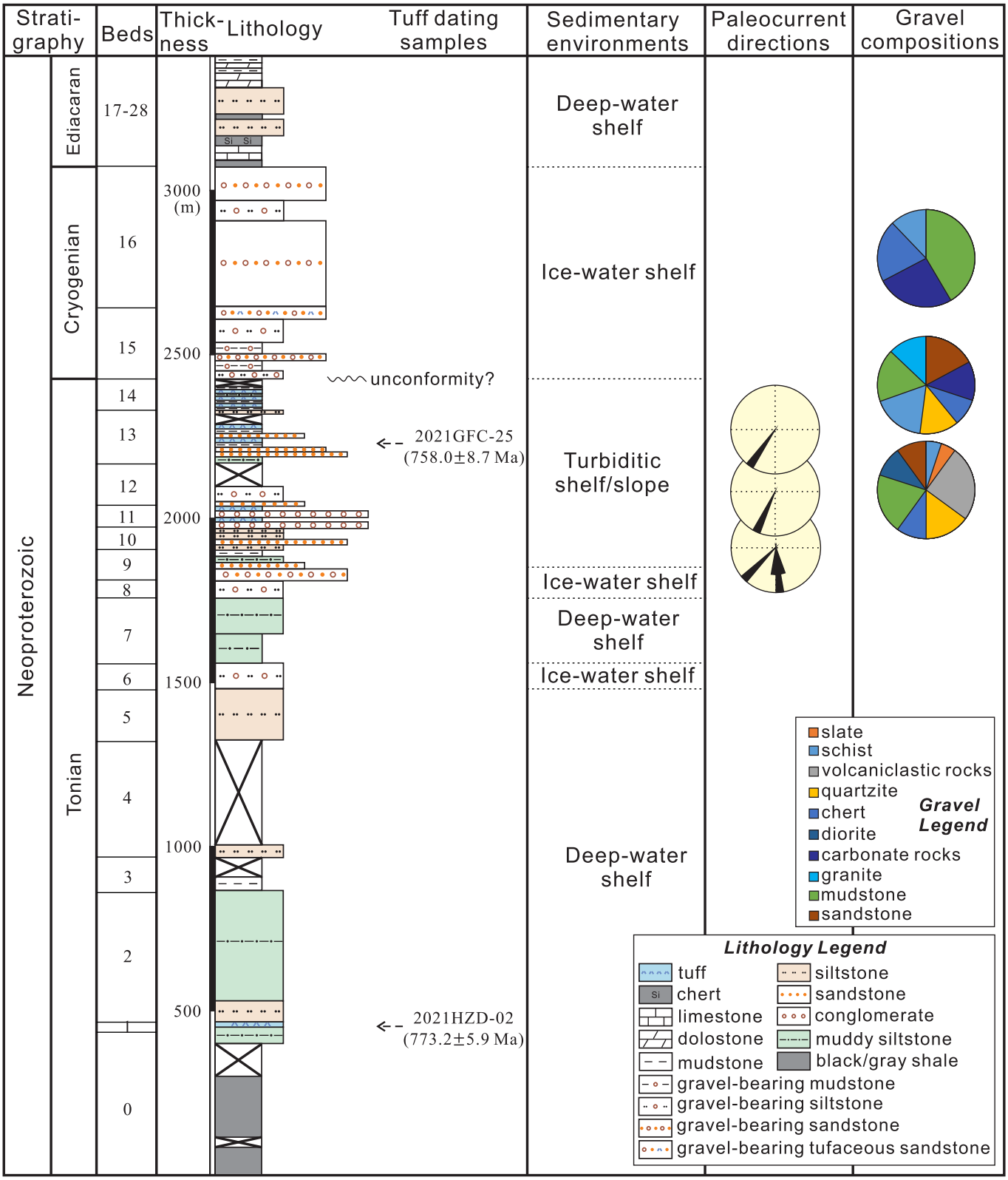

Fig. 3. Outcrop lithology, sedimentary environments and field-based paleocurrent orientation and gravel composition data from the Neoproterozoic strata at the Gaofengcun section. Note that the paleocurrent orientations were only obtained from the turbiditic strata.

observed for those representative transparent heavy minerals.

3.2.4. Whole-rock major-, trace- and rare earth element analyses

Whole-rock major and trace elemental compositions were conducted at the Analytical Laboratory, Beijing Research Institute of Uranium Geology. Samples were crushed and powered to less than 200 meshes for elemental analyses. The Loss on ignition (LOI) values were obtained by measuring the weight loss after heating the sample powders at 980 °C. Whole-rock major element analyses were measured using an Axios-mAX X-ray fluorescence spectrometer (XRF). Trace elements (rare earth

elements included) were analyzed using an Element XR Inductively Coupled Plasma Mass Spectrometer (ICP-MS). Both precision and accuracy were better than 5% and 10% for major and trace elements, respectively.

4. Results

4.1. Zircon U-Pb ages

Zircons from all the samples are euhedral prismatic grains, with oscillatory growth zoning, typical of magmatic zircon. The SHRIMP U-Pb dating results of samples 2021HZD-02, 2021GFC-25, and 2021GFC-12 are illustrated in Fig. 4A-C, while the LA-ICP-MS U-Pb dating results for the sample 21GFC-32 are illustrated in Fig. 4D. All the raw dating data are shown in Tables A1 and A2 in the supplemental materials.

Nineteen grains from sample 2021HZD-02 were analyzed and available sixteen spots yield a mean $^{206}Pb/^{238}U$ age of 773.2 ± 5.9 Ma (Fig. 4A). Three grains with ages of 805.9 ± 11.2, 818.0 ± 10.9, and 861.3 ± 11.8 Ma show discordance to the main population and the concordia line, which may be attributed to the mix of older zircons along with the volcanic tuffs. Therefore, the three ages were removed in the calculation of the mean age. For sample 2021GFC-25, twenty grains were analyzed and eight spots yield a mean $^{206}Pb/^{238}U$ age of 758.0 ± 8.7 Ma (Fig. 4B). The other twelve spots have age duration from 793.7 ± 10.8 to 918.0 ± 12.4 Ma with a mean age of 849.1 Ma, which are most likely derived from older zircons together with the deposition of volcanic tuffs. Twelve grains were analyzed for sample 2021GFC-12. The usable eleven spots therein yield a weighted mean $^{206}Pb/^{238}U$ age of 798.3 ± 8.5 Ma with a single age population (Fig. 4C). A total of 104 detrital zircon grains from sample 21GFC-32 were analyzed and the age spectra are dominated by a strong peak at ca. 750 Ma, with minor Mesoproterozoic and Paleoproterozoic ages (Fig. 4D).

4.2. Sedimentological and petrographic features

Representative outcrop photographs of the Gaofengcun section are shown in Figs. 5–7. Descriptions of the stratigraphic column (Fig. 3) from the bottom to the top are as follows. the Bed 0 is about 480 m in thickness and mainly comprises black and gray laminated shales, silty mudstones and subordinate massive muddy siltstones (upper parts of this bed). These fine-grained sedimentary rocks are rich in horizontal millimeter to centimeter-scale laminae (Fig. 5A–B) and have been

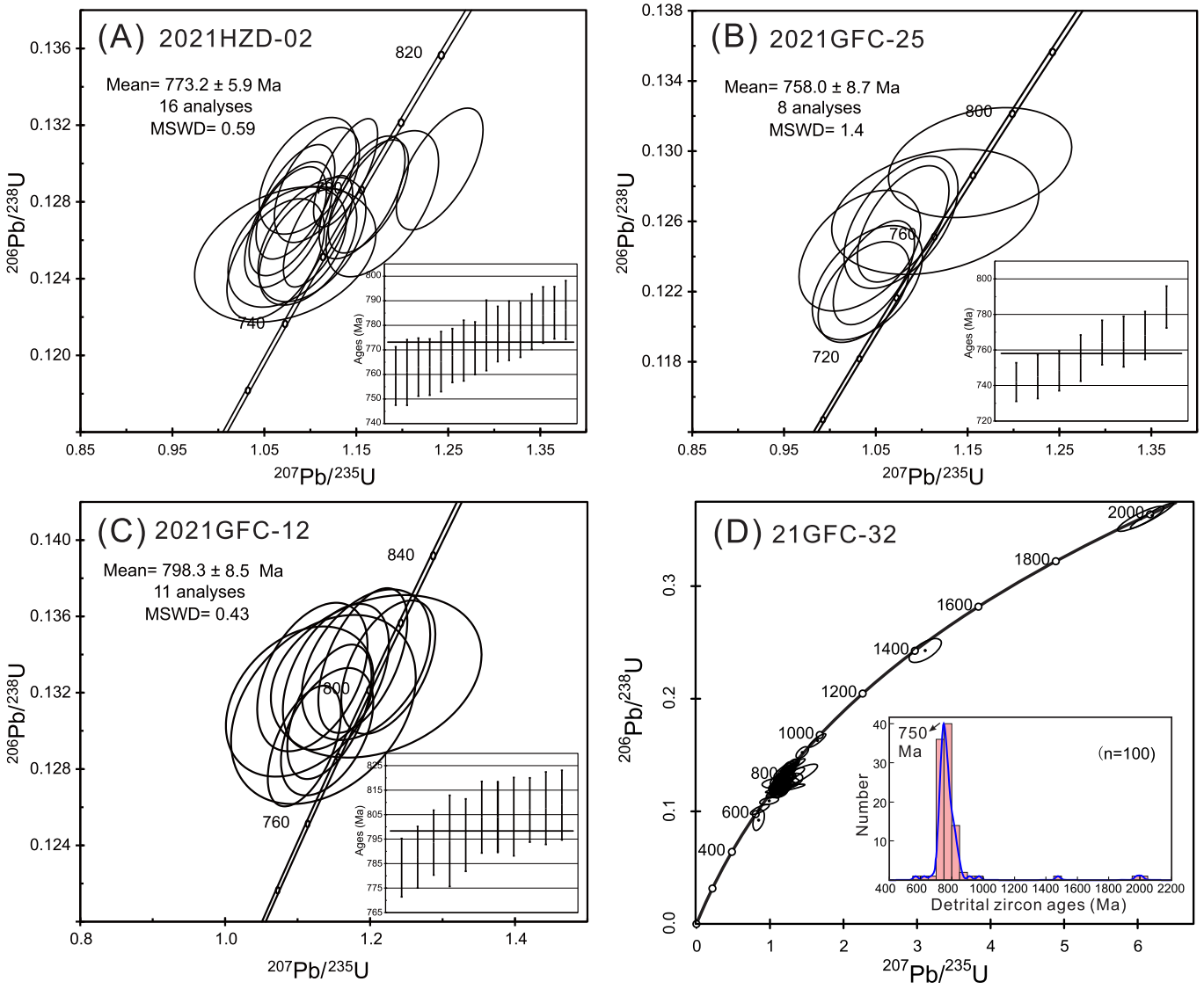

Fig. 4. Zircon U-Pb dating results of the analyzed samples, including the U-Pb concordia diagrams and weighted average U-Pb ages for volcanic tuffaceous samples 2021HZD-02 (A) and 2021GFC-25(B), granite gravel sample 2021GFC-12(C) and the detrital zircon U-Pb Concordia ages and Kernel density estimation (KDE) plots (by using bandwidth = 15 in the DensityPlotter program (Vermeesch, 2012)) for sample 21GFC-32 (D).

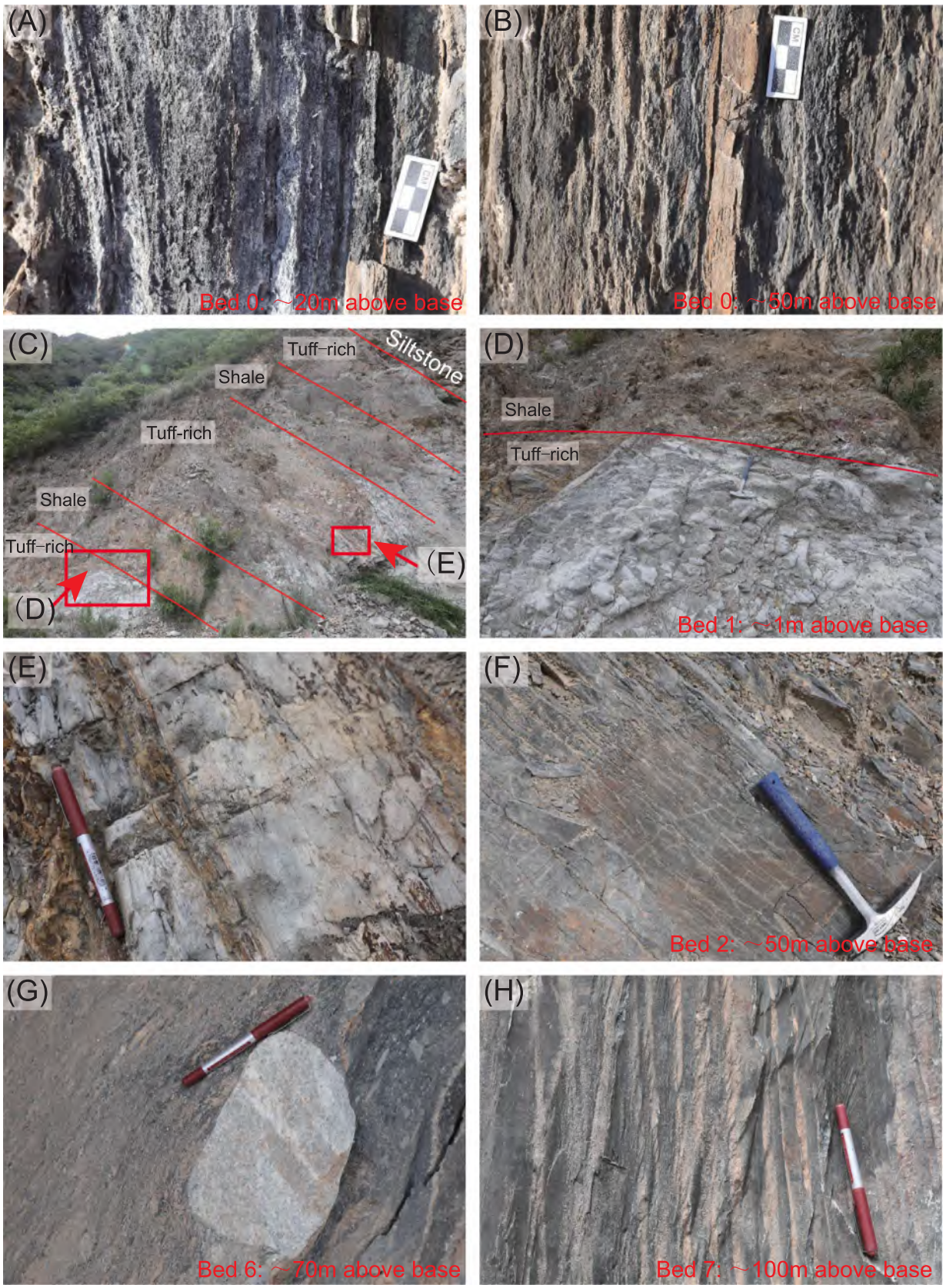

Fig. 5. Representative outcrop photographs and sedimentological features of the lower part strata at the Gaofengcun section. (A)–(B): slightly metamorphosed, laminated fine-grained sedimentary rocks; (C)–(E): tuffaceous rocks interbedded with shales; (F): siltstone strata; (G): ice-water deposits with poorly-sorted dropstone gravels; (H): laminated deep-water fine-grained rocks.

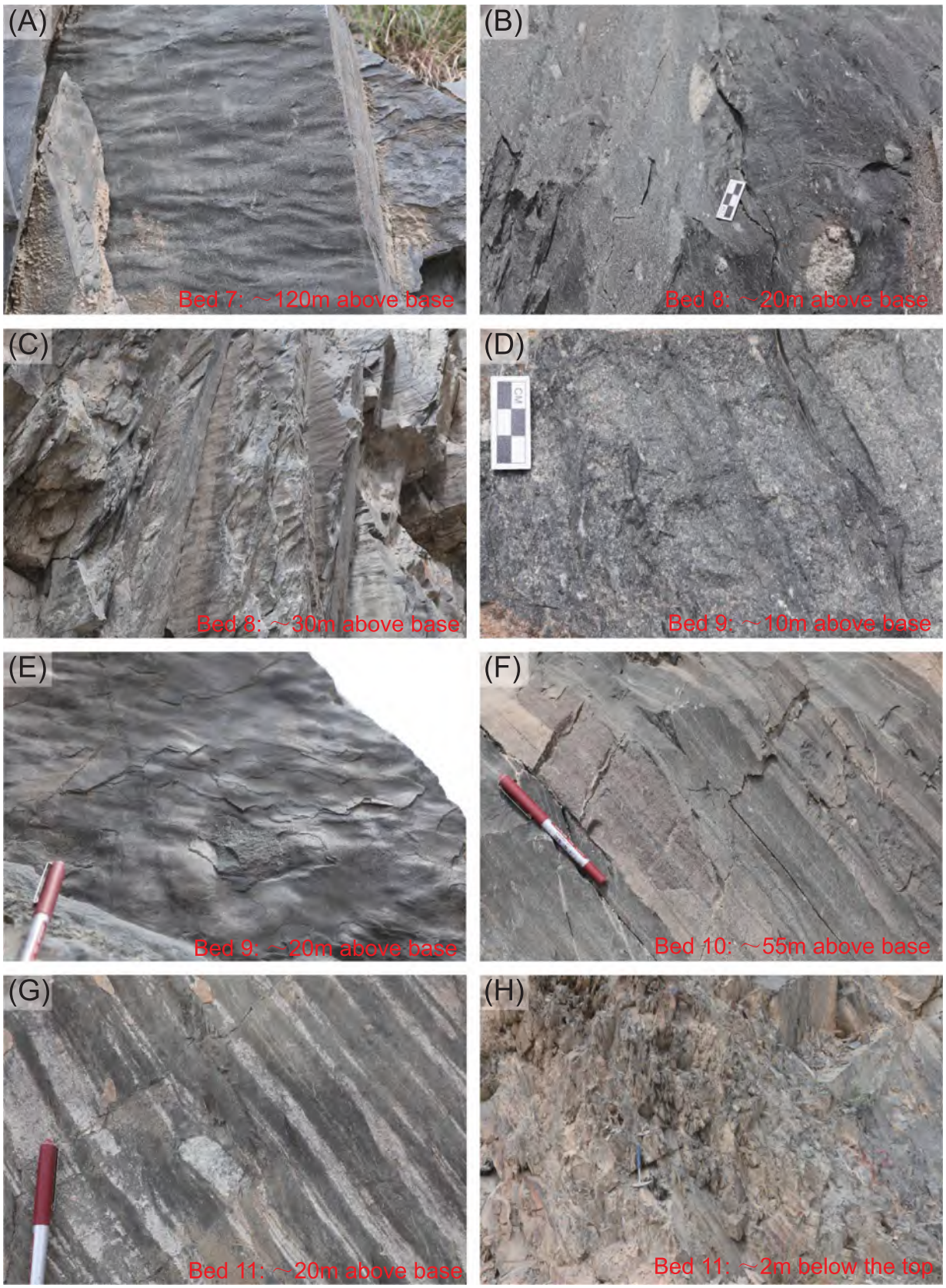

Fig. 6. Representative outcrop photographs and sedimentological features of the middle part strata at the Gaofengcun section. (A): ripples of deep-water deposits; (B) glacial diamictites with dropstone textures; (C) laminated shales with ripples; (D) massive turbiditic sandstone strata; (E) flute casts; (F) parallel bedding siltstone and mustone strata; (G)–(H): fine-grained turbiditic strata with dropstone gravels.

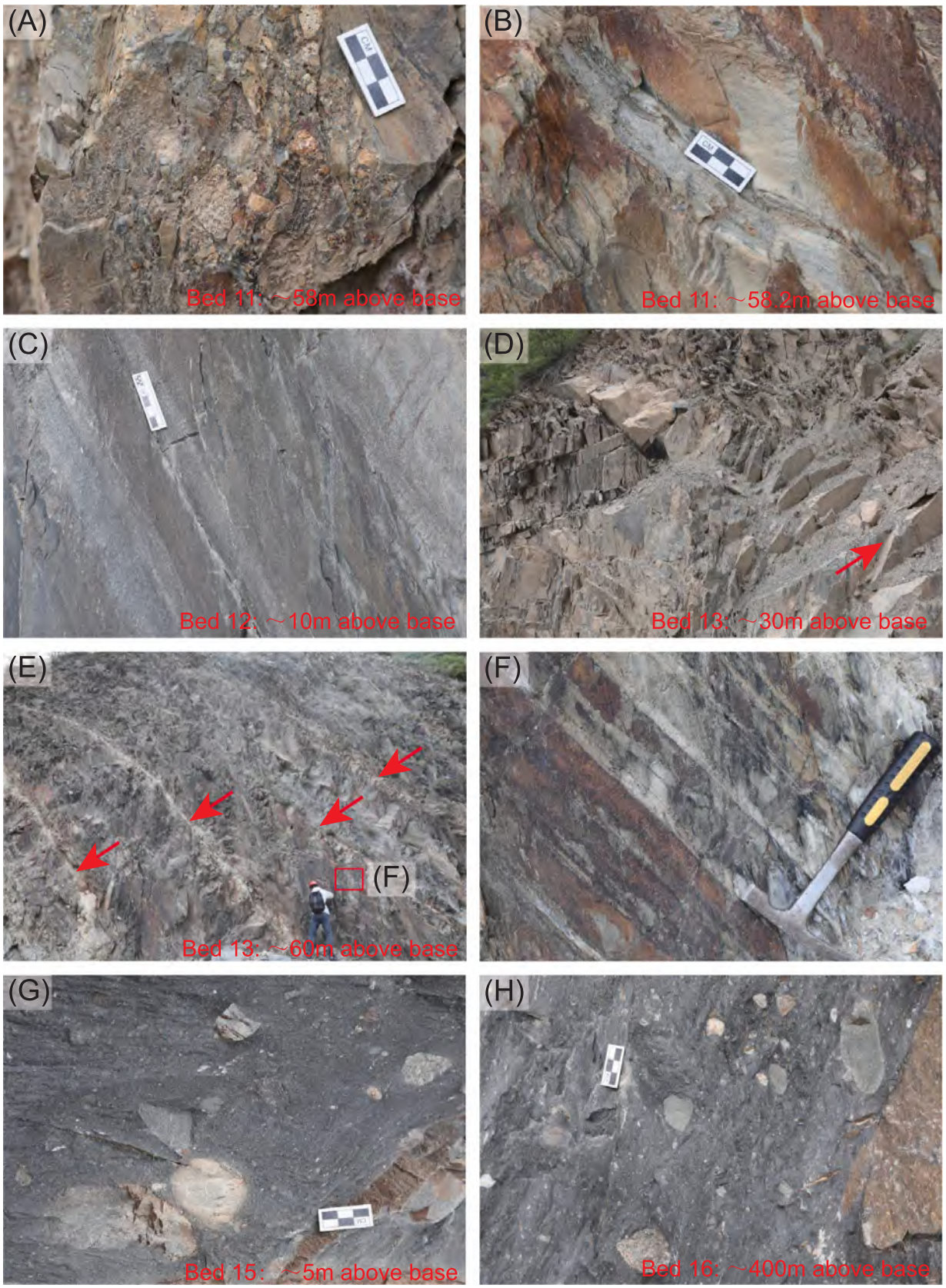

Fig. 7. Representative outcrop photographs and sedimentological features of the middle part strata at the Gaofengcun section. (A)–(B): basal conglomerates, sandstones and siltstones of a turbiditic succession; (C): siltstones and mudstones; (D)–(F): fine-grained strata with tuffaceous interbeds; (G)–(H): gravel-rich glacial diamictites.

slightly metamorphosed. The Bed 1 is composed of thin interbeds with tuff-rich layers and shales (Fig. 5C–E). the Beds 2–5 and Bed 7 mainly consist of thick-bedded siltstones and silty mudstones (Fig. 5F and 6A) and several parts therein are covered by plants or slope protection materials. The Beds 6 and 8 comprise gravel-bearing siltstones (Fig. 5G and 6B). The gravels therein are poorly-sorted and are characterized by quartzite, granitoid rocks and sedimentary rocks. The Bed 9 is dominated by an upward-fining sequence with gravel-bearing coarse-grained sandstones at the bottom, parallel bedding fine-grained to medium sandstones in the middle and siltstones and mudstones at the top (Fig. 6D–E). Typical sedimentary structures also include ripples, cross bedding and flute casts. The Beds 10–14 comprise similar sedimentary records to the Bed 9, with several thin volcanic tuffaceous rock interbeds (Fig. 6F–H and 7A–F). The Beds 15–16 represent ca. 600 m thick diamictite strata, including matrix-supported conglomerates, gravel-rich sandstones and siltstones. These gravels are poorly-sorted and compositionally-diverse (Fig. 7G–H). The Beds 17–28 represent as Ediacaran sedimentary strata with black shales, limestones, cherts and siltstones at the bottom, and dolomite and subordinate mudstones at the top (Fig. 3).

Paleocurrent orientations were mainly determined by pebble-cobble imbrications, ripples, sandstone lens and flute casts from the turbidite strata. Valid measurement results demonstrate dominant southwest- and south-directed paleoflow (Fig. 3). The diamictite strata have abundant, diverse gravels (Figs. 5–7). The gravels are poorly sorted and mainly range from 4 mm to 20 cm in sizes. The gravel clasts dominantly involve sandstone, mudstone, quartzite, schist and granite, with subordinate slate, chert, diorite and carbonate and volcaniclastic rocks (Fig. 3).

Both outcrop and microscopic features indicate that the lower part strata have been slightly metamorphosed (Fig. 5; Fig. 8). The sandstones from Beds 9–14 are mainly grain-supported and moderately to poorly sorted (Fig. 9A–B), whereas the diamictite samples from Beds 15–16 are typically matrix-supported and poorly sorted (Fig. 9C–E). Shapes of the detrital grains are diverse, including angular to rounded grains. Most of the analyzed petrographic samples are greywacke (litharenite). These samples are rich in sedimentary lithic fragments (17–58%, such as mudstone, sandstone and carbonate rocks) and quartz grains (8–54%) and are comparatively poor in feldspar grains (2–27%) (Table A3; Fig. 9). The modal data indicate that the Tonian samples are plotted in the recycled orogenic and arc fields in the Dickinson (1985) ternary diagram based on framework grain compositions (Q-F-L) (Fig. 10A), while most of the analyzed Cryogenian samples are plotted in the recycled field. Two samples have very high lithic fragment contents and are plotted in the undissected arc field in this ternary diagram (Fig. 10A). The point-counting detrital grains from these two samples are relatively coarse (rich in gravel grains). The framework grain compositions are distinctly variable vertically (Fig. 11), especially for those Tonian samples. Although the lithic fragments in most samples are dominated by sedimentary fragments, some samples are also relatively rich in metamorphic and volcanic fragments (>10%) (Fig. 11).

4.3. Heavy minerals

The transparent heavy minerals in the analyzed Neoproterozoic sedimentary rocks mainly include zircon, chlorite, tourmaline, epidote, with minor rutile, hornblende, biotite and barite (Table A4). These heavy mineral grains are poorly sorted and are angular to rounded in shape (Fig. 10C). For instance, detrital zircons, acting as one of the major

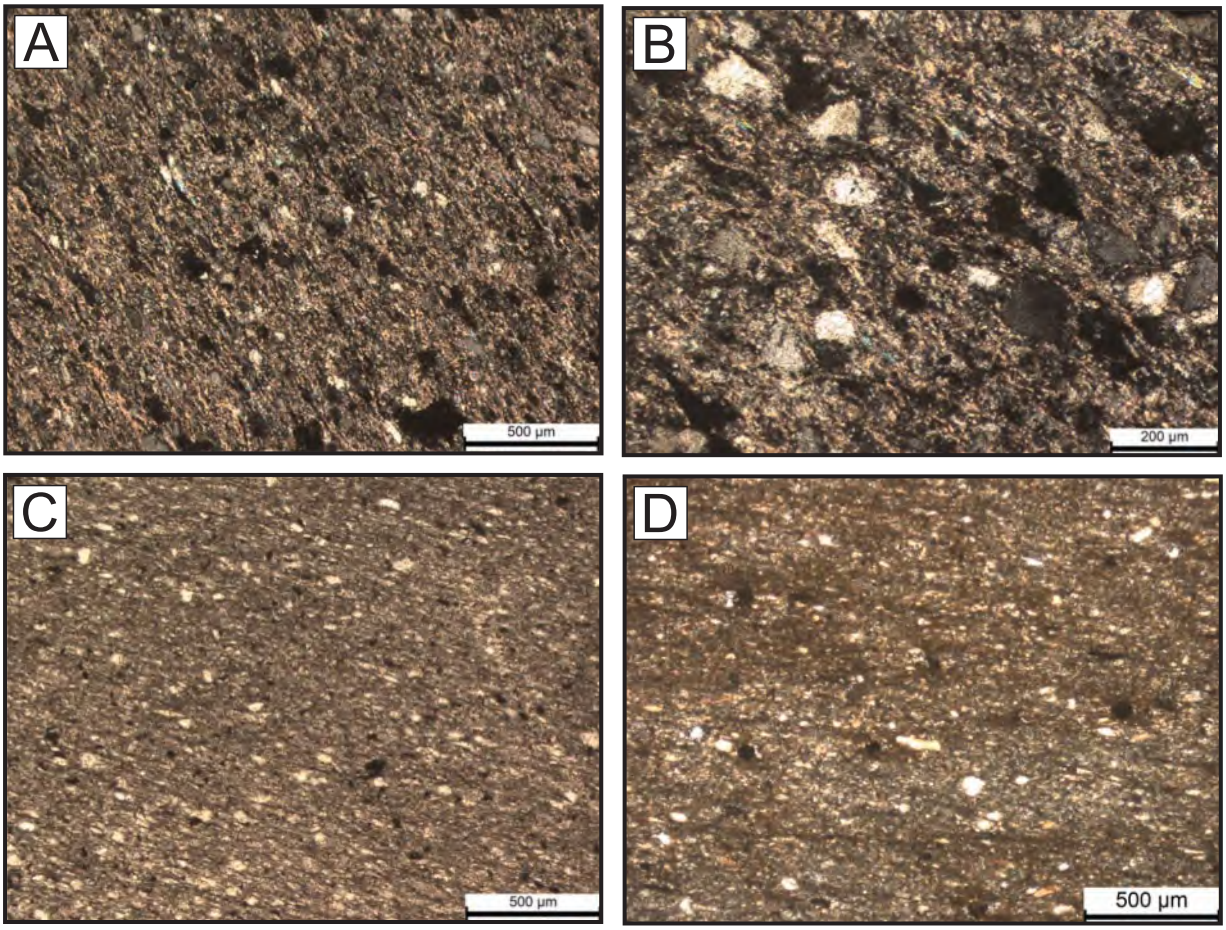

Fig. 8. Representative micrographs of the Neoproterozoic fine-grained sedimentary rocks from the investigated Gaofengcun section. (A) and (B) sample 21GFC-12, slightly metamorphosed silty mudstone, characterized by mud matrix sericitization; (C) sample 2021GFC-18; (D) sample 21SC-44.

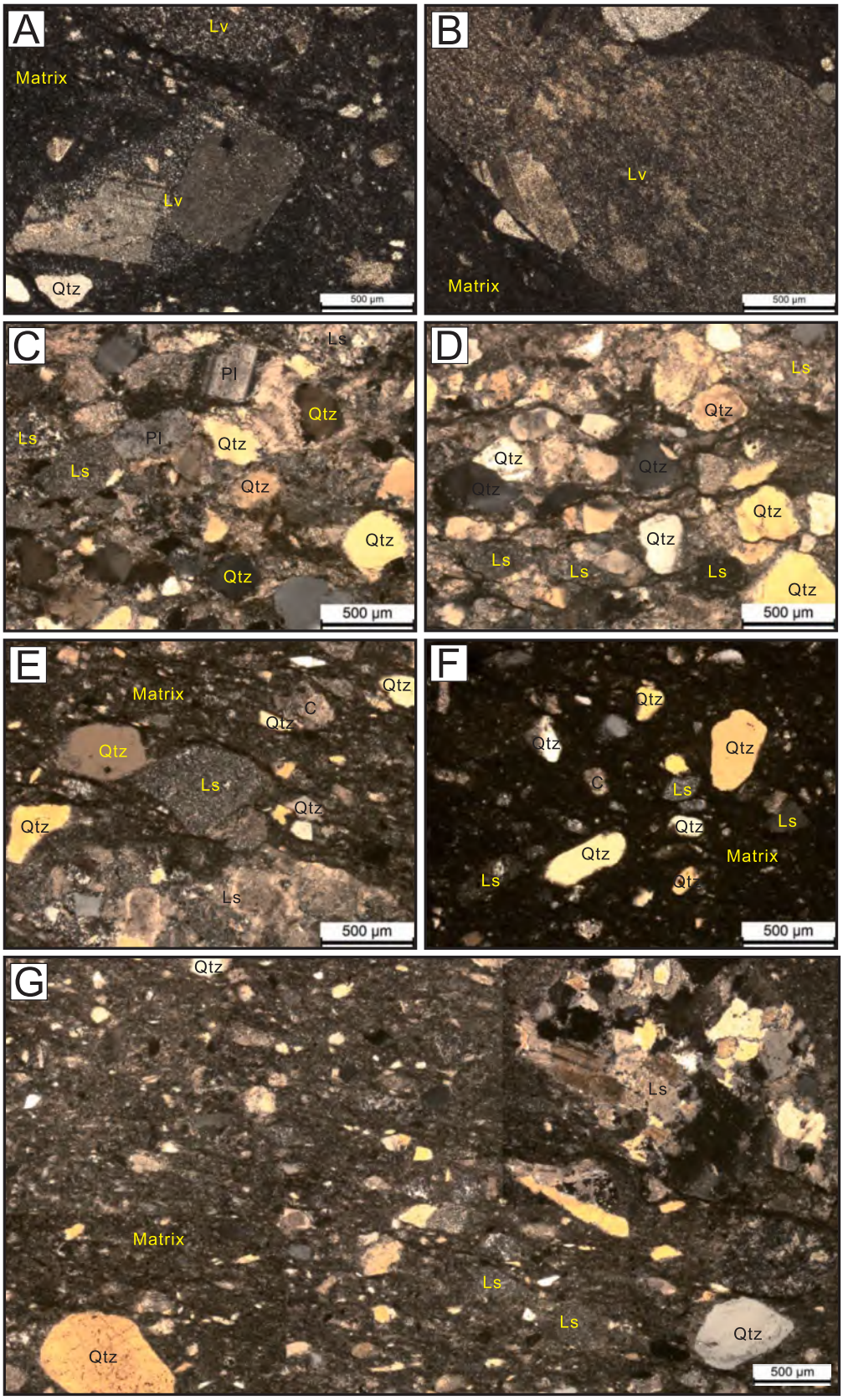

Fig. 9. Representative micrographs of the Neoproterozoic sand-size sedimentary rocks from the Gaofengcun section. (A)–(B) samples 21-GFC-25 and 2021GFC-11, Tonian diamictite with volcanic lithic fragments; (C)–(D) samples 21SC-54 and 21SC-61, Tonian turbidite sandstones; (E)–(G) samples 21SC-64, 21SC-76 and 21SC-71, Cryogenian diamictite (poorly-sorted graywacke). Qtz: quartz; Pl: plagioclase; Lv: volcanic lithic fragment; Ls: sedimentary lithic fragment; C: carbonate.

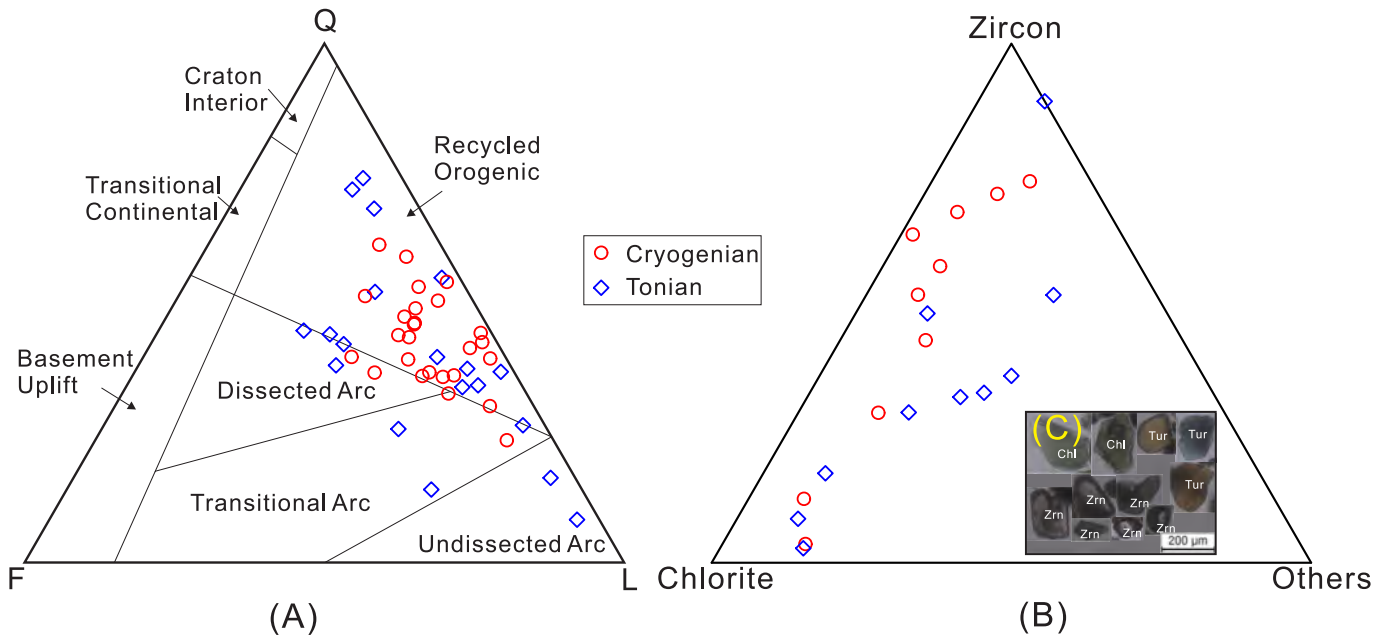

Fig. 10. (A) Quartz-Feldspar-lithic fragment (Q-F-L) ternary plots of the analyzed sandstone samples. The tectonic background interpretations are from Dickinson (1985). (B) Transparent heavy mineral composition ternary plots. The end-member "Others" includes tourmaline, rutile, epidote, hornblende, biotite and barite. (C) Representative micrographs of the heavy mineral grains (from sample 21SC-69, Cryogenian diamictite), Zrn: zircon; Tur: tourmaline; Chl: chlorite.

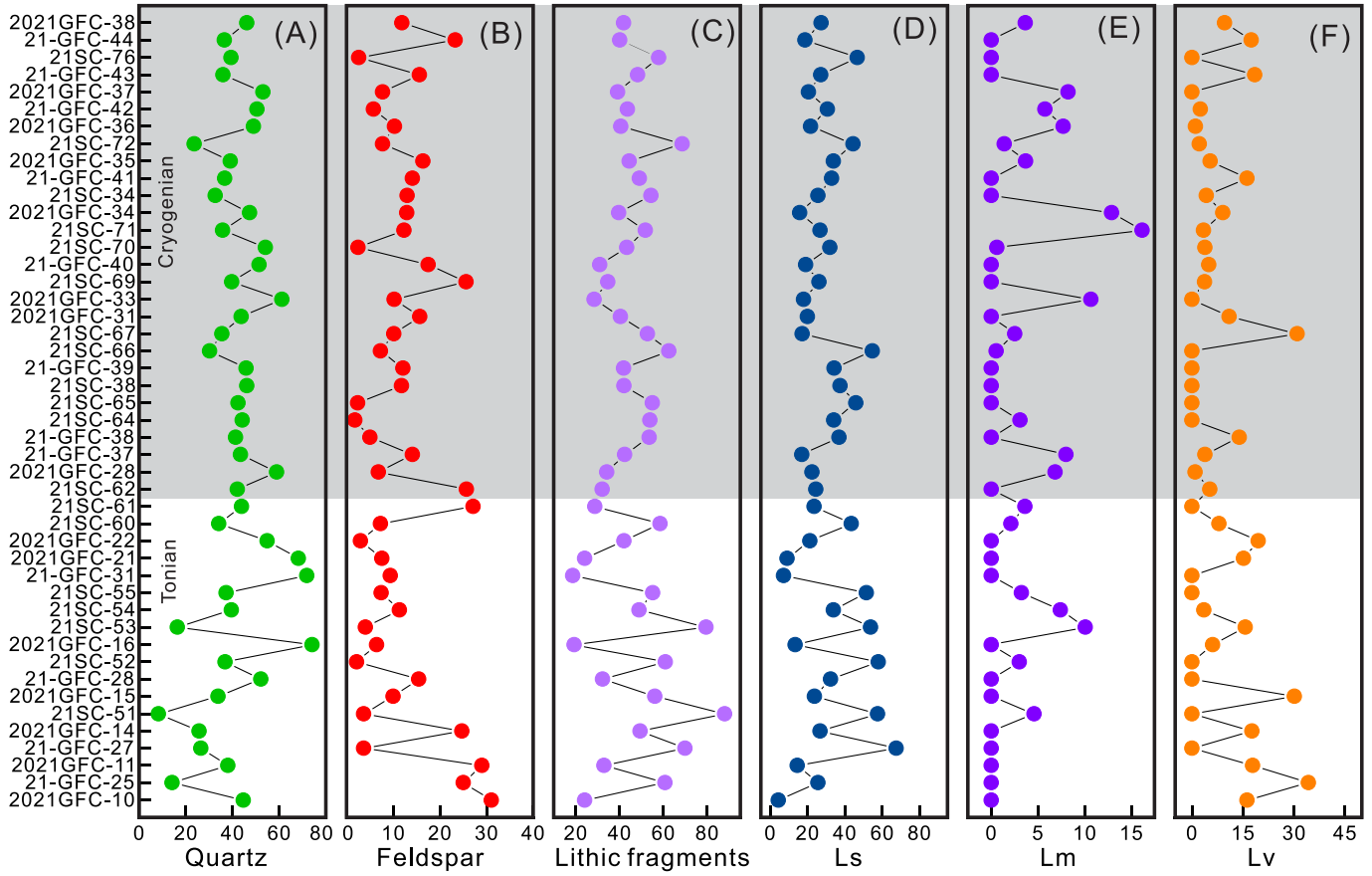

Fig. 11. Vertical variations in framework grain compositions of the analyzed samples from the Gaofengcun section. Ls (sedimentary lithic fragment), Lm (metamorphic lithic fragment) and Lv (volcanic lithic fragment) indicate percentage values of those in all the counted framework grains.

heavy minerals (3–89% in total transparent heavy minerals), appear as euhedral, subhedral and rounded and ranges from 30 to 400 μm. The analyzed samples indicate quite diverse heavy mineral assemblages (Fig. 10B) and variable ZTR index (proportions of zircon, tourmaline and rutile in all transparent heavy minerals, proposed by Hubert (1962), indicating compositional maturity) values (Fig. 12). Several samples

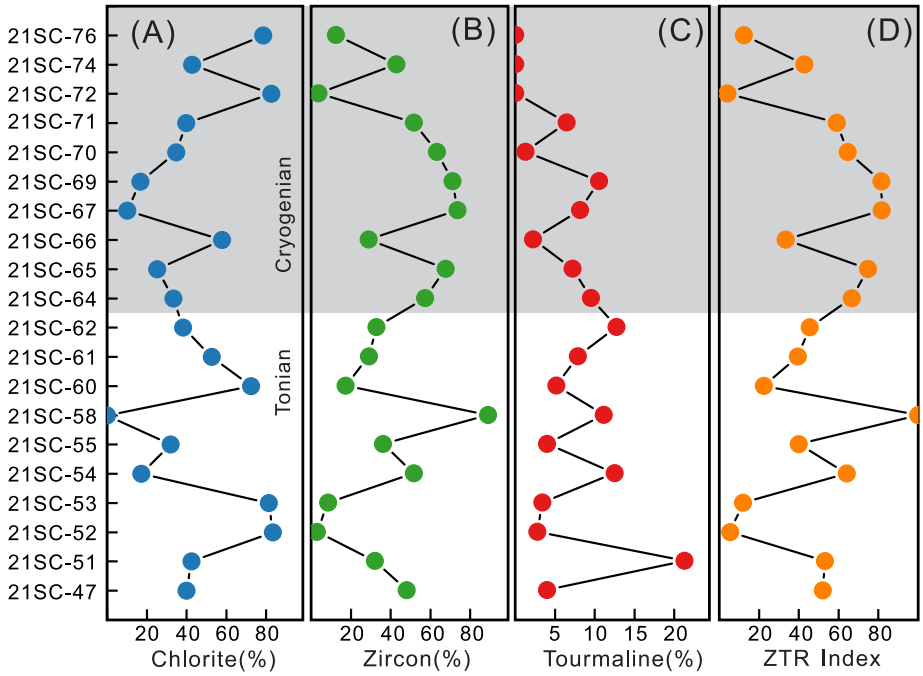

Fig. 12. Vertical variations in major transparent heavy mineral compositions of the analyzed samples from the Gaofengcun section. ZTR Index = 100 × (zircon + tourmaline + rutile)/all transparent heavy minerals (Jian et al., 2020b, 2023).

have high chlorite contents (up to 80%) and relatively high tourmaline contents (up to 20%) (Fig. 12). Stratigraphically, these are not any predictable variation trends for both each mineral composition and the ZTR index values (Fig. 12).

4.4. Major-, trace- and rare earth element composition

All the raw element geochemical data are shown in Table A5–A7 in the supplemental materials. Element concentrations of all the analyzed samples were normalized to the Upper Continental Crust (UCC) compositions and are shown in Fig. 13. The results indicate that some samples exhibit marked depletion in Ca, Pb, Sr, Ni and light rare earth elements (LREEs) relative to UCC (Fig. 13). The UCC-normalized REE patterns show that the LREEs are relatively depleted, compared with heavy rare earth elements (HREEs) for most samples. The chondrite-normalized REE patterns are shown in Fig. 14. The results demonstrate that all the samples show LREEs enrichment. Most samples exhibit flat patterns for middle and heavy rare earth elements with variable Eu anomaly values (Fig. 14), but some samples (especially some Tonian samples, Fig. 14A) indicate relative depletion of middle rare earth elements. Major element-based sediment chemical weathering intensity evaluation (A-CN-K ternary plot) results show that all the analyzed samples are plotted along the ideal weathering trend parallel to the A-CN axis (Fig. 15). Vertical variations of the representative element ratios and chemical weathering index values are illustrated in Fig. 16. The major element-based chemical weathering intensity induces, such as the Na/Al, CIA and PIA values, are quite variable and range from 0.1 to 0.5, from 50 to 75 and from 50 to 85 (Fig. 16), respectively. The Th/Sc and La/Th ratios, which are commonly used to indicate sediment parent-rock compositional variations, range from 0.2 to 0.6 and from 0.5 to 10 (Fig. 16), respectively. Stratigraphically, the Cryogenian samples have much lower CIA and PIA values and comparatively higher Na/Al ratios, than the Tonian samples. The Tonian samples indicate variable elemental ratio values (such as Th/Sc, La/Th, $La_{(CN)}/Yb_{(CN)}$ and Eu anomaly values), whereas the Cryogenian samples show relatively consistent elemental ratio values (Fig. 16; Fig. 17). Most samples are plotted in the felsic and mixed felsic-mafic source field in the La/Th-Hf binary diagram (Fig. 17A) and a few Tonian samples have comparatively high Zr and Hf contents, revealing marked signals of old sediment recycling (Fig. 17). The La-Th-Sc and Th-Sc-Zr/10 ternary plots are shown in Fig. 18 and indicate that most samples are plotted in the "continental island arc" field with minor samples in the "oceanic island arc" field (Fig. 18).

5. Discussion

5.1. Depositional ages of the Gaofengcun section and comparison with equivalent Tonian–Cryogenian sequences in the Yangtze Block

Investigations on the well-exposed Neoproterozoic clastic strata at the Gaofengcun section have not been reported. The equivalent sedimentary succession has been defined as the Guanjiagou Formation at the Guanjiagou section (Fig. 2A) in the direct north of Wenxian City, approximately 20 km west of the Gaofengcun section. Most researchers considered the Guanjiagou Formation as being younger than the Hengdan Group and older than the Ediacaran strata (Druschke et al., 2006; Lu et al., 2006). Some researchers considered it to be deposited during the Nantuo period (late Cryogenian) due to the features of glacial deposits (i.e., Marinoan glaciation; ca. 650 to 635 Ma; Su et al., 2003; Wang et al., 2010; Gao et al., 2020a). Furthermore, the Guanjiagou Formation was also given as a Late Triassic (ca. 220 Ma) depositional age based on the $^{40}Ar/^{39}Ar$ dating method (Yan et al., 2004b).

In this study, we measured the section (Fig. 2B) in the northwest limb of the Gaofengcun anticline, which records an overall coarsening-upward sedimentary succession (Fig. 3), from thin-bedded mudstone to diamictite-dominated deposits. The SHRIMP zircon U-Pb dating from the thick volcanic tuffaceous layer (i.e., sample 2021HZD-02), near the lowest part of the section, yields a weighted average age of 773.2 ± 5.9 Ma, which represents the approximately early-stage depositional age of this clastic succession. The dating results are consistent with the end age of Tonian arc volcanic activities (846–776 Ma) in the Bikou terrane reported by Yan et al. (2004a) and are also consistent with the peak age of detrital zircon grains from the Hengdan Group reported by Druschke et al. (2006). The SHRIMP age of 758.0 ± 8.7 Ma from the thin-bedded volcanic tuffaceous layers (i.e., sample 2021GFC-25) in the middle part of the section, although influenced by older detritus, indicates a younger

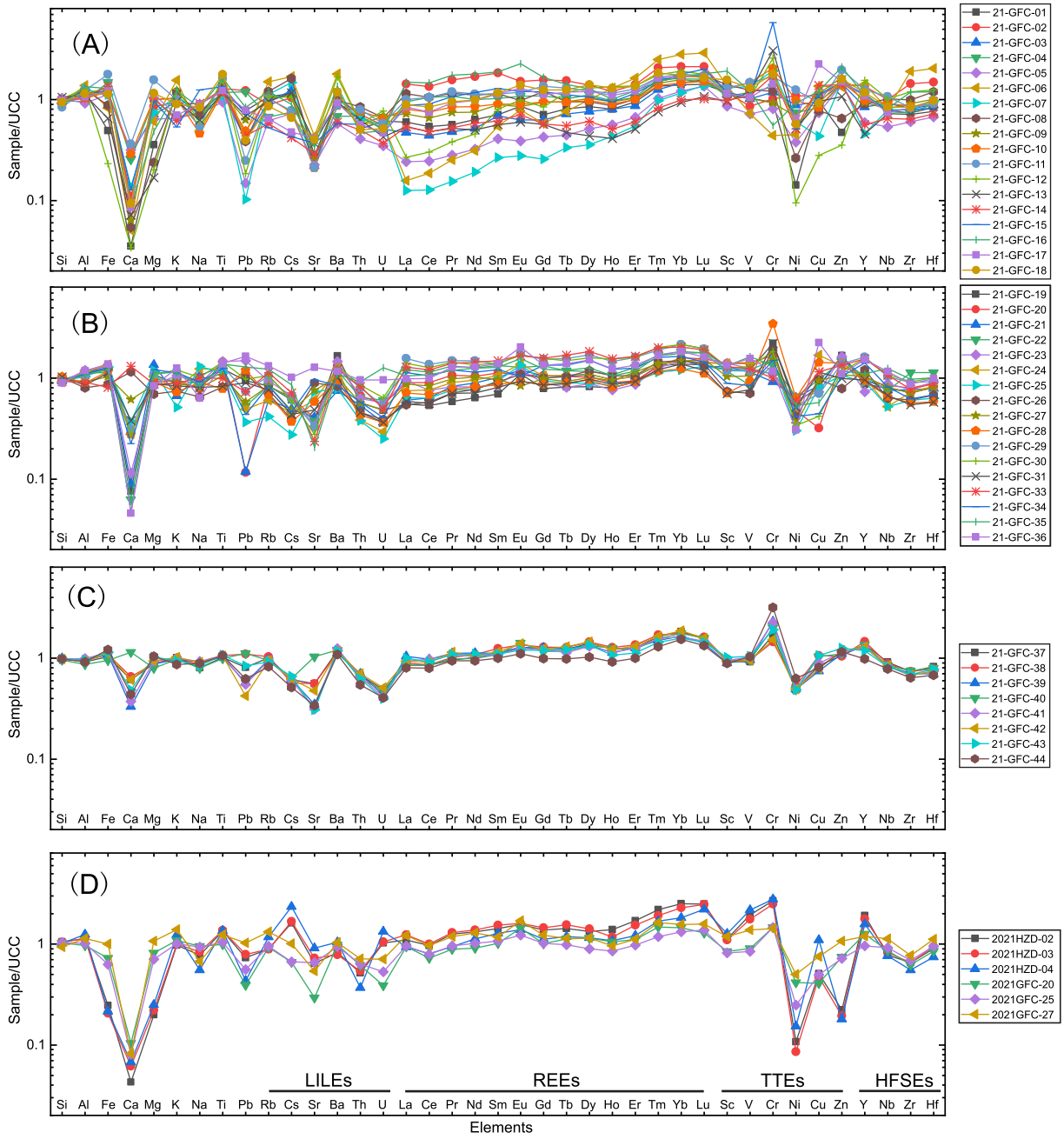

Fig. 13. Major and trace element geochemical results of all the analyzed samples. All the element data were normalized by the Upper Continental Crust (UCC) compositions. (A)–(B) Tonian samples; (C) Cryogenian samples; (D) volcanic tuffaceous rocks. The UCC data are from Rudnick and Gao (2014). LILEs: large ion lithophile elements; REEs: rare earth elements; TTEs: transition trace elements; HFSEs: high field strength elements.

depositional age than the basal deposits. As for the granite gravel (2021GFC-12) sample, the SHRIMP age of 798.3 ± 8.5 Ma is coincident with the age duration of the Bikou Group volcanic rock associations (i.e., 846–776 Ma; Yan et al., 2004a). In addition, the detrital zircon ages obtained in this study (sample 21GFC-32) show a peak age of ca. 750 Ma, revealing the maximum depositional ages for the dated strata, which is also consistent with the peak age of the detrital zircons from the Hengdan Group strata (Druschke et al., 2006; Wu et al., 2019) and the end age of the Tonian Bikou terrane volcanic activities (Yan et al., 2004). These ages are consistent with the depositional time of the Liantuo Formation (and its equivalent formations) in South China (Wang et al., 2003; Du et al., 2013; Lan et al., 2015; Pi and Jiang, 2016; Yang et al., 2022). The stratigraphic division and correlation of the Liantuo Formation and its equivalent formations have been a hot, critical topic in Neoproterozoic studies on the Yangtze Block. Although the Liantuo Formation was previously considered as the lower part of Nanhua system (i.e., Cryogenian) in some early literatures (e.g., Yin et al., 2003; Wang et al., 2006; Liu et al., 2008), most Radiometric dates from tuff/tuffaceous beds within the Liantuo Formation suggest it was deposited in a time interval of ca. 780–714 Ma (Lan et al., 2015 and references therein). The Tonian and Cryogenian periods were recommended as 1000 Ma to 720 Ma and 720 Ma to 635 Ma in the newest Geologic Time Scale (v. 6.0; Walker and Geissmaet al., 2022), respectively. Therefore, we agree the current, widely-accepted proposition that the Liantuo Formation and its equivalent formations belong to the Tonian period, rather than the Cryogenian period (e.g., Chen et al., 2021; Yang et al., 2022).

The top thick diamictite-dominated glacial deposits (Beds 15–16,

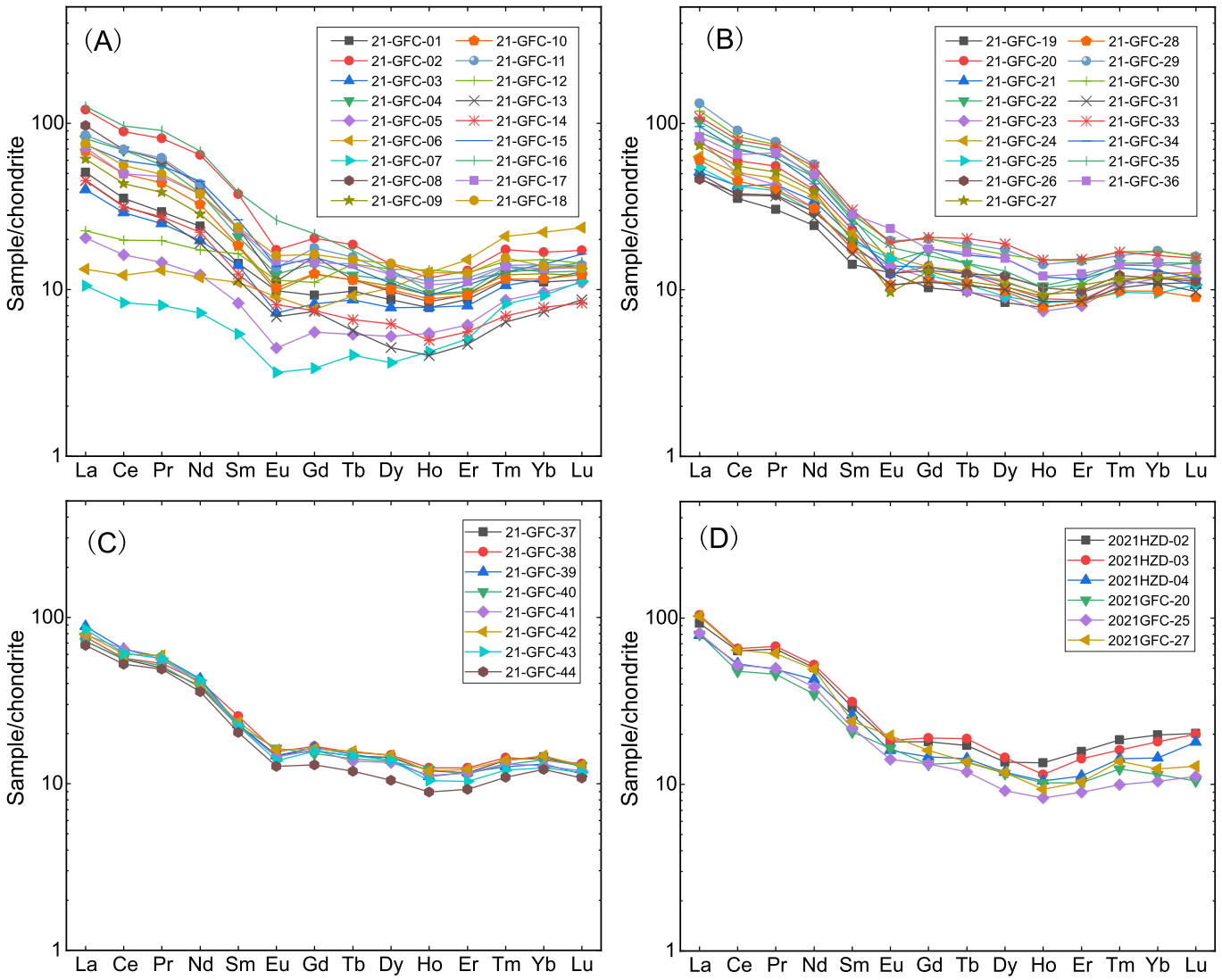

Fig. 14. Chondrite-normalized REE patterns of the analyzed fine-grained sedimentary rocks from the outcrop section. The chondrite data are from McDonough and Sun (1995). (A)–(B) Tonian samples; (C) Cryogenian samples; (D) volcanic tuffaceous rocks.

Fig. 3) at this section are continuous and conformably overlain by Ediacaran strata (Fig. 2B), which is coincident with that in most regions of the Yangtze Block (Gu et al., 2023). We suggest these glacial diamictite strata might be well correlated with the Cryogenian (720–635 Ma) records (i.e., the Nanhua system in Chinese geological documents). It is well known that there were two stages of glaciation during the Cryogenian, i.e., Sturtian (ca. 720–659 Ma) and Marinoan (ca. 650–635 Ma) glaciations, corresponding to the Chang'an and Gucheng Formations (or their equivalent formations) and the Nantuo Formation in the Yangtze Block (Qi et al., 2020; Chen et al., 2021), respectively. Here, the glaciation stage for the thick glacial deposits (i.e., Beds 15–16) is not clear due to the absence of volcanic tuffaceous layers. Further detailed investigations focusing on the diamictite strata are important to better understand the relationships between Cryogenian records in the Bikou terrane and global glacial events. Although absolute ages between the dated younger volcanic tuffaceous bed (ca. 758 Ma) and the thick glacial deposits were not obtained, we infer that this interval may be between 758 and 720 Ma.

Collectively, this section shows Neoproterozoic clastic successions from the middle–late Tonian to Cryogenian (ca. 773–635 Ma). We note that there is a ubiquitous unconformity between the Tonian (i.e., Qingbaikou system) and Cryogenian (i.e., Nanhua system) sedimentary records in South China (Lang et al., 2018; Yang et al., 2022). However, the unconformity is not clear at the Gaofengcun section (the top parts of the Bed 14 at the outcrop section are covered (Fig. 3)). The present study was just a preliminary attempt to unravel the depositional time of the thick strata and further high-resolution dates are required for better determination of the depositional ages of the sedimentary records in this region.

5.2. *Tonian–Cryogenian depositional environment evolution*

While previous studies have suggested that most regions of the Neoproterozoic Yangtze Block were in terrestrial, shelf and slope-basin environments (Jiang et al., 2011; Bao et al., 2018; Lang et al., 2018; Yang et al., 2022), the investigated outcrop section indicates diverse sedimentary rock assemblages (Figs. 5–7) from the bottom-up, implying remarkable variations in sedimentary environments over time. The lower parts of the Tonian strata are mainly composed of black and gray laminated shales, silty mudstones and subordinate massive muddy siltstones, with couples of tuffaceous rock interbeds (Fig. 5). These fine-grained sedimentary rocks are featured by horizontal millimeter to centimeter-scale laminae and are suggested to form in low-energy hydrodynamic conditions. We infer that these fine-grained rocks were deposited deep-water shelf environments (Fig. 3). The middle parts of the Tonian strata comprise massive siltstones and greywackes, with

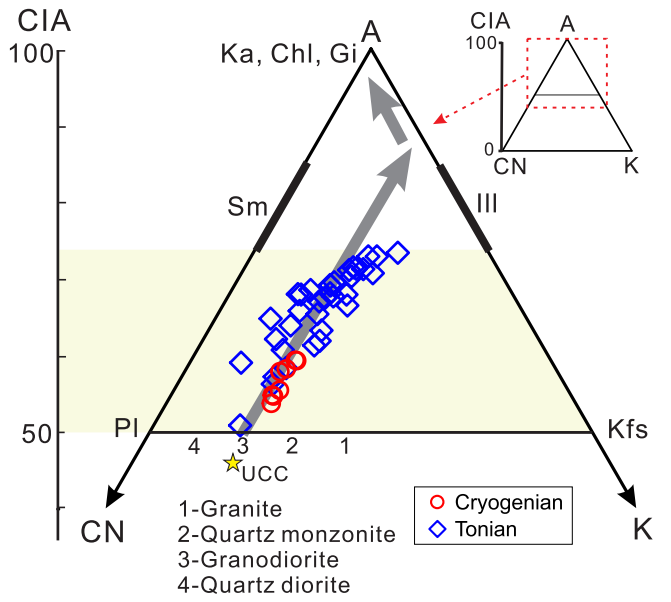

Fig. 15. A-CN-K (Al_2O_3-CaO + NaO_2-K_2O) ternary plots of the analyzed fine-grained sedimentary rocks from the investigated outcrop section. The gray lines with arrows indicate ideal weathering trends (modified from Jian et al. (2013) and Fu et al. (2022)). The results indicate that these sedimentary rocks represent weathering residues and products from the source terranes where mild–moderate chemical weathering occurred, i.e., within the plagioclase-weathering stage (Jian et al., 2019b; Mei et al., 2021). The Cryogenian sediments have relatively lower CIA values than those Tonian sediments, revealing obvious climate variations during the middle–late Neoproterozoic. Note that if the analyzed sedimentary rocks were influenced by diagenetic K-metasomatism, the K-addition would result in decrease of CIA values and deviation from the ideal weathering trends (toward to K-apex in the A-CN-K diagram for clay-rich mudstones) (Fedo et al., 1995; Jian et al., 2013). Our results indicate little effects of diagenetic K-metasomatism. Granite, quartz monzonite, granodiorite and quartz diorite and UCC data were from Fu et al. (2022). Ka: Kaolinite; Chl: Chlorite; Gi: Gibbsite; Sm: Smectite; Ill: Illite; Pl: Plagioclase; Kfs: K-feldspar; UCC: Upper Continental Crust.

gravel-bearing, coarse-grained rock intervals (Figs. 5–6). These gravels are highly poorly-sorted, matrix-supported and non-oriented and are thus expected to have distinct transport agents from the silt-dominated matrix. We suggest that these are of glacial origin, rather than submarine fan origin as previously reported (Su et al., 2003; Yan et al., 2004; Lu et al., 2005). The megaclast-bearing, matrix-supported rocks show dropstone textures which can be best explained by glacial marine sedimentation (Condon et al., 2002; Rodríguez-López et al., 2016; Le Heron et al., 2017). And the megaclasts were most likely ice-rafted detritus, rather than deep-water gravity flow deposits. We favor that these glacial diamictites were most likely deposited in an ice-water shelf. The fine-grained deposits within dropstone-rich intervals demonstrate that the ice-water and deep-water environments occurred alternately during this period (Fig. 3) and the dropstone intervals record episodic ice-rafting events analogous to the Pleistocene Heinrich events of the North Atlantic (Heinrich, 1988). The upper parts of the Tonian strata are composed of dropstone-free, turbidite-like deposits, characterized by incomplete bouma sequences, with several tuffaceous layers. Sedimentary structural features include massive graded coarse-grained sandstones with gavels at base, flute casts, ripples, plane parallel laminae and horizontal silty and muddy laminations (Figs. 6–7). We favor that these strata can be interpreted as deposits in turbiditic shelf/slope environments (Fig. 3). By contrast, the ~600 m Cryogenian strata in the upper part of this section are dominantly composed of megaclast-bearing, glacial diamictites where dropstone textures frequently appear, revealing ice-water shelf sedimentary environments for a long time.

Chemical weathering intensity indicated by siliciclastic sedimentary rocks is commonly applied to discuss paleo-weathering and paleo-climate evolution of the sediment source-to-sink systems (e.g., Jian et al., 2013; Zhao and Zheng, 2015; Fu et al., 2022). Several major element-based indices, such as CIA, CIW, PIA and Na/Al ratios (Fig. 16), have been widely applied to quantitatively evaluate chemical weathering intensity of sedimentary rocks. We have realized that these bulk-rock geochemical indices might be influenced by hydrodynamic sorting (grain-size effects) and post-K metasomatism (e.g., conversion of kaolinite to illite) processes (Fedo et al., 1995; Jian et al., 2013). Our new data indicate that most samples are plotted close to the ideal weathering trends in the A-CN-K ternary diagram (Fig. 15) and the CIA values are highly correlated with the CIW and PIA values (Fig. A1 in the supplemental figures), implying little effects of diagenetic K- metasomatism. Only fine-grained samples were selected for elemental geochemical analysis in this study, signifying minor interferences from grain sizes. The weathering index values and their temporal variations (Figs. 15–16) in this study match well with the lithofacies and sedimentary environment explanations above. Specifically, the deposits of ice-shelf environments have much lower CIA (53–62 and 58–74 for glacial and non-glacial sediments, respectively) and PIA (55–64 and 65–85) values and higher Na/Al values (0.28–0.44 and 0.12–0.40) than those deep-water and turbiditic sediments (Fig. 16), reflecting mild weathering intensity in the sediment source-to-sink process during the ice ages and moderate weathering during the non-glacial periods. Our results, documented in the Bikou terrane, are consistent with those of previous studies on other regions in the Yangtze Block (e.g., Deru et al., 2007; Wang and Zhou, 2013; Huang et al., 2016; Ai et al., 2020; Gao et al., 2020a; Qi et al., 2020). Mean annual temperature estimations based on Na chemical depletion index (i.e., τNa-MAT transfer function) show ca. 20 ± 5.4 °C temperature differential between Cryogenian cryochron and nonglacial interlude, revealing distinct surface climate conditions and variable sedimentary environments during the Neoproterozoic glacial-interglacial cycles (Qi et al., 2020).

5.3. Sedimentary provenance interpretations

Gravel compositions in the glacial diamictites can directly indicate parent-rock types in sediment source terranes. The field-based clast counting results demonstrate diverse parent-rocks, including mudstones, sandstones, volcaniclastic rocks, quartzite, granite, schist and chert. Petrographic analysis results of the sandstone and greywacke samples also display dominant detritus supply of sedimentary parent-rocks and detrital quartz of igneous origin (Fig. 9). Although transparent heavy minerals are relatively scarce, the available grains appear as both first-cycle and recycled heavy minerals (Fig. 10). All the results reveal predominant erosion of felsic parent-rocks, most likely from crystalline basement rocks and sedimentary cover from the adjacent continents.

We note that some Tonian diamictite samples have relatively high contents of feldspar grains and volcanic lithic fragments (Fig. 9 A-B) and the model analysis data reveal their sources within arc-related settings (Fig. 10A). This is consistent with the compositions of the Tonian dropstones in gravel-bearing diamictite strata which are rich in volcaniclastic rocks (Fig. 3). We favor that the Tonian strata were fed by mixed bedrock associations of both arc and recycled orogenic origin. By contrast, the Cryogenian strata were dominantly derived from orogenic sources. The felsic bedrock-dominated source parent-rock interpretations are also supported by element geochemical data of the analyzed mudstone samples (Fig. 13), although these fine-grained fractions might have different sources and transport agents with those ice-rafted detritus. Our new detrital zircon dating data (Fig. 4D) and the previously reported detrital zircon U-Pb geochronological data of the Neoproterozoic sedimentary strata (e.g., the Bikou and Hengdan Group) in the Bikou terrane demonstrate overwhelmingly dominance of 720–950 Ma ages (Druschke et al., 2006; Gao et al., 2020a, 2020b; Hui et al., 2021; Mao et al., 2021).The early to middle Neoproterozoic

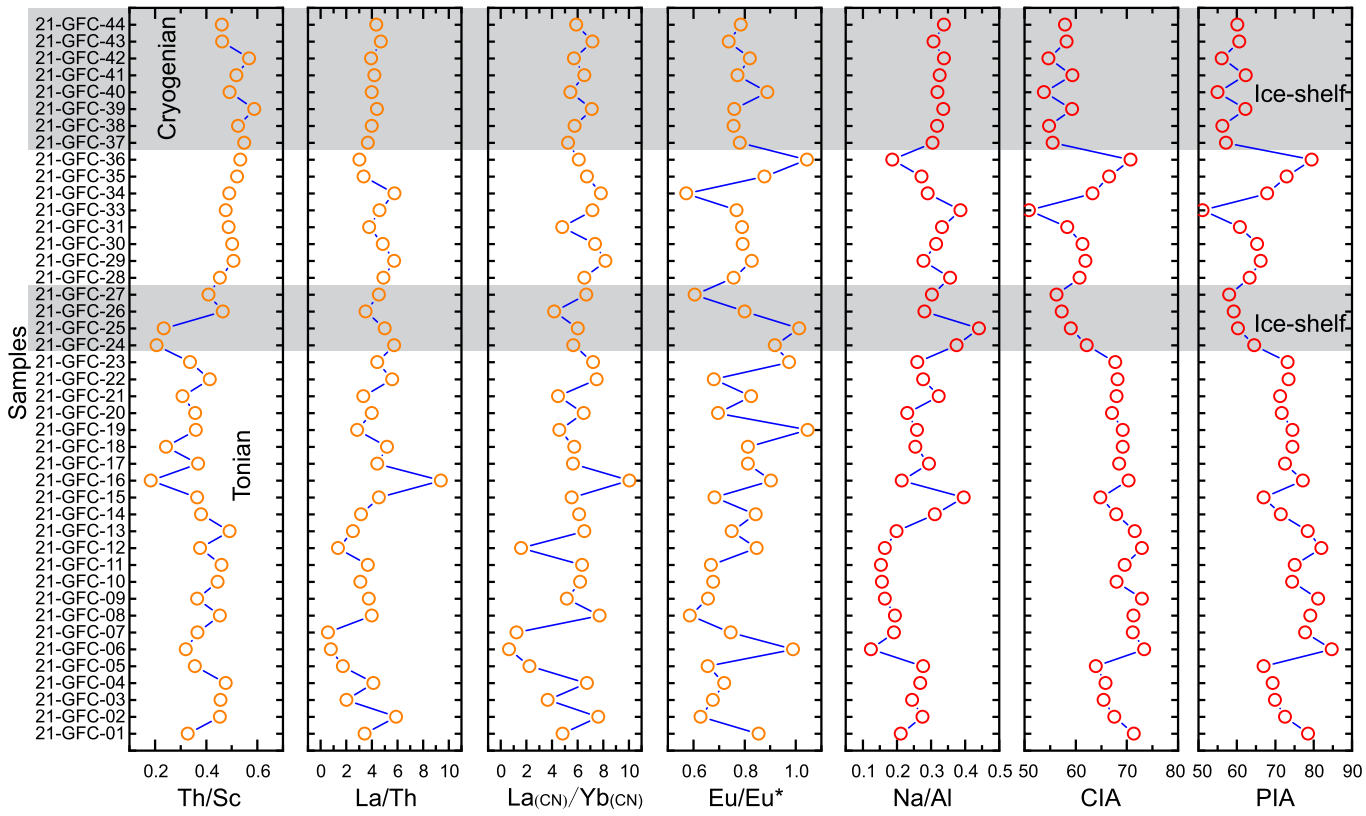

Fig. 16. Vertical variations of Representative element ratios and chemical weathering intensity proxies. $La_{(CN)}/Yb_{(CN)}$ represent as the ratio of Chondrite-normalized values and indicates differentiation degrees between light and heavy rare earth elements. Eu/Eu* represents Eu anomaly and indicates negative Eu anomalies when the values < 1. CIA values = $[Al_2O_3/(Al_2O_3 + CaO^* + Na_2O + K_2O) * 100]$ in molecular proportions (Jian et al., 2013), where CaO* represents CaO content in the silicate fraction. PIA values = $[(Al_2O_3–K_2O)/(Al_2O_3 + CaO^*+Na_2O–K_2O) * 100]$. The gray bands indicate samples of ice-shelf environments.

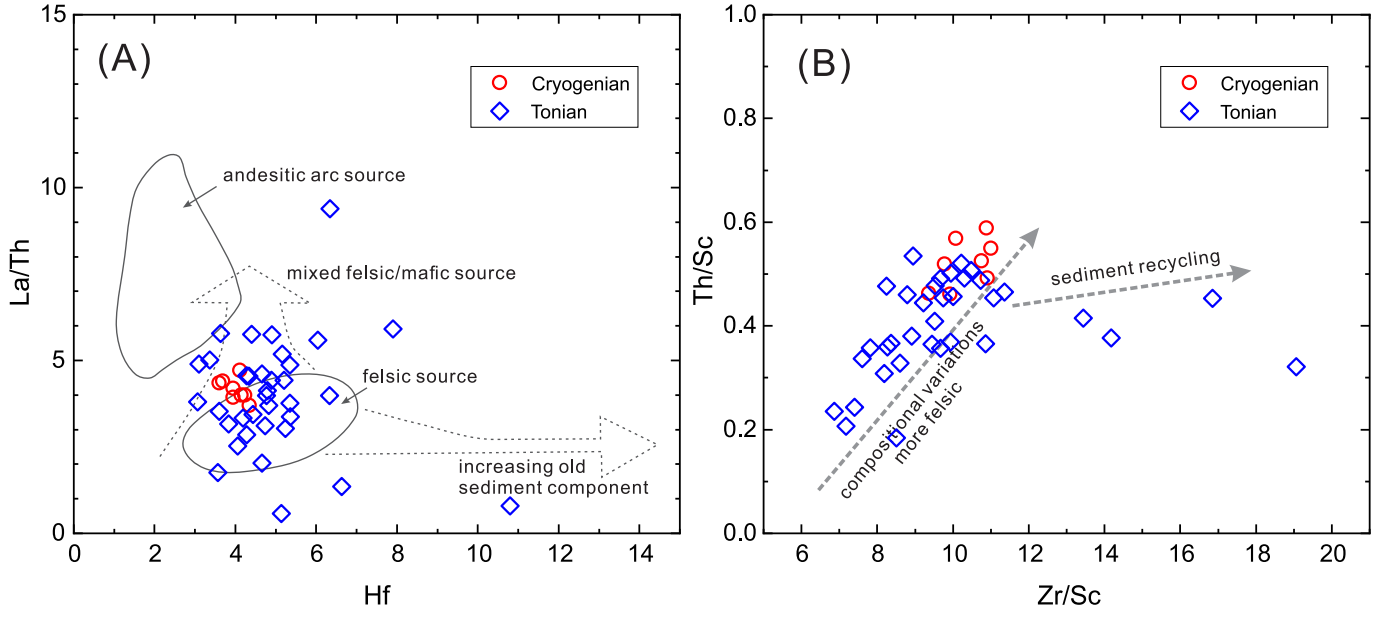

Fig. 17. Representative trace element ratio binary diagrams for the analyzed samples. (A) La/Th vs. Hf (after Floyd and Leveridge, 1987); (B) Th/Sc and Zr/Sc (after McLennan et al., 1993; Jian et al., 2020b).

detrital zircon signals are also dominant prominent in Neoproterozoic strata from the northern and western Yangtze Block (e.g., Wang et al., 2010, 2012, 2013; Cui et al., 2014; Li et al., 2020; Wang et al., 2023), revealing that these detrital zircon grains were most likely fed by similar early to middle Neoproterozoic igneous rock-dominated source terranes. Previous investigations demonstrate that felsic igneous rocks with early to middle Neoproterozoic ages are widespread in Bikou and western Yangtze regions (Sun et al., 2008, 2009; Wang et al., 2012; Gao et al., 2020a and reference therein). Given that the investigated Neoproterozoic sedimentary rocks indicate low textural and compositional

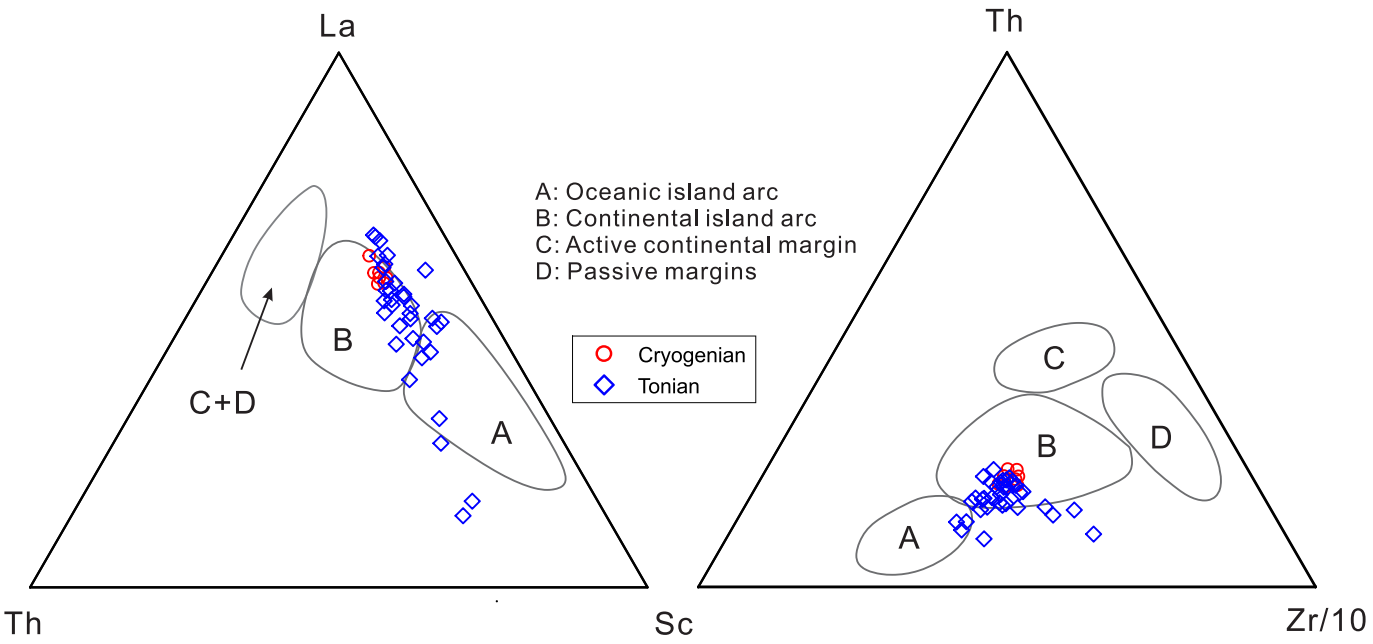

Fig. 18. Fine-grained sedimentary rock trace element-based tectonic setting interpretations (after Bhatia and Crook, 1986) for the investigated Gaofengcun section.

maturity, we advocate that the analyzed Neoproterozoic sedimentary rocks (including detrital zircon grains therein) were sourced from the pre-middle Neoproterozoic sedimentary and metasedimentary successions and the early to middle Neoproterozoic arc-origin acidic to intermediate igneous rocks in the Bikou terrane and the western Yangtze Block to the east (the current orientation), rather than previously suggested distant continental blocks in the Rodinia supercontinent (e.g., Eastern India-East Antarctica, Yu et al., 2008).

Our new results demonstrate that the provenance indicators of the analyzed Neoproterozoic sandstones, such as the petrographic and heavy mineral compositions, display obviously vertical variations (Fig. 10), which is different from those elemental proxies of the fine-grained samples. The unpredictable variation trends imply that it is hard attributed to dramatic changes in source regions, but rather to overall low, highly varied transport abilities of the agents (i.e., ice and water) under the changing climate conditions. These vertical variations and possibly insufficient sediment supply also signify an under-compensated depositional process in ice-water and deep-water environments.

5.4. Tectonic implications

It has long been hotly debated with respect to the origin and tectonic setting of the Bikou terrane during the Neoproterozoic, and consequently two conflicting views have been proposed, i.e., a continental/island arc setting (Yan et al., 2004; Druschke et al., 2006) or a continental rift setting (Xia et al., 1999; Xu et al., 2002) as described above. From the perspective of global plate reconstruction, the present-day consensus is that the South China Craton occupies a peripheral position of the northwestern margin of the Rodinia supercontinent (Yan et al., 2004a; Druschke et al., 2006; Gao et al., 2020b). In this case, the Yangtze Block faced to an open ocean during the Neoproterozoic time. Most researchers considered the Bikou terrane as the most northwestern isolated portion of the Yangtze Block (Yan et al., 2003; Druschke et al., 2006; Gao et al., 2020a; Hui et al., 2021). However, we favor that the West Qinling and Bikou terranes geographically connected with the Yangtze Block, rather than isolated microterranes during the middle Neoproterozoic time. We drew the conclusion because we found a similar Neoproterozoic sedimentary assemblage at the Baiyigou section in the West Qinling orogen based on field observations (unpublished results). This proposition is consistent with the concept of Neoproterozoic "Greater South China Block" which might involve the Kunlun, Qaidam and Qilian terranes (currently in the northern Tibetan Plateau) (Jian et al., 2020a) and even more terranes related to the northwestern India (Wang et al., 2021).

Our new sedimentological, petrographic, geochemical, and U-Pb isotopic data also provide insight into the Neoproterozoic tectonic settings of the Bikou terrane. The dominant immature components in the analyzed Tonian sandstone samples, especially the occurrence of volcanic fragments, indicate non-ignorable contributions from a proximal arc-related source (Fig. 10A). However, the signals of volcanic fragments and arc sources are rarely present in the analyzed Cryogenian samples, suggesting obvious variations in sediment source terranes or in tectonic settings. The age spectra of detrital zircons from the upper section show a prominent peak age at ca. 750 Ma which is close to the depositional time (Fig. 4D), revealing a possible convergent plate margin setting for the depositional regions (Cawood et al., 2012). In addition, both the La-Th-Sc and the Th-Sc-Zr/10 ternary plot results (Fig. 18) indicate that these fine-grained sedimentary rocks were most likely related to sources of continental arcs with minor components of island arcs.

Except the Bikou Group volcanic rocks (ca. 846–776 Ma), some older volcanic rocks (ca. 970 Ma) have been reported in the Jiaoziding complex by Li et al. (2018). Some older plutons (ca. 880 Ma) have been reported in the Bikou terrane (Xiao et al., 2007). Similar plutons (ca. 880 Ma) were recently found in the Liujiaping complex in the present-day Longmenshan fold-thrust belt (Hui et al., 2021). These volcanic rocks and plutons were thought to be generated in a subduction-related arc setting (Xiao et al., 2007; Li et al., 2018; Hui et al., 2021). In conclusion, we favor that, during the early-middle Neoproterozoic (ca. 970–750), these microterranes (e.g., the West Qinling and Bikou terranes) were located in the margin of the Yangtze Block under convergent settings, experienced subduction and collision and subsequently formed continental arcs and orogens. After that, the tectonic settings in these regions might be extensional and the Yangtze Block was then in a passive margin.

6. Conclusions

In this contribution, we focus on a well-exposed, 3000 m-thick Neoproterozoic sedimentary outcrop section (named as Gaofengcun section) in the northwestern Bikou terrane, NW Yangtze Block and present integrated investigation results combining field-based sedimentology, petrography, zircon U-Pb geochronology and elemental geochemistry. This study yields the following conclusions.

1) Based on the volcanic tuffaceous rock U-Pb dating data and stratigraphic correlation results, depositional ages of the Gaofengcun section can be constrained to be late Tonian period for the lower parts and Cryogenian period for the upper parts, as the equivalents to the widespread Liantuo Formation and the Nanhua system (Cryogenian) in the Yangtze Block, respectively.
2) This section represents an overall coarsening-upward succession, from deep-water sequences to ice-water glacial diamictite sequences with dropstone textures. Although the compositions of the analyzed Neoproterozoic succession are variable stratigraphically, we favor that the Tonian deposits were most likely fed by mixed sources with arc-related terranes and recycled orogenic terranes, whereas the Cryogenian deposits were dominated by detritus from recycled orogenic terranes. We suggest the nearby felsic arc granitoid rocks, volcanic rocks, sedimentary cover and basement crystalline rocks as major parent-rocks for the deposits. In addition to the temporal variations in tectonic settings and source terranes, the changing climatic conditions, which dominated the sediment transport agents and abilities, might play a crucial role in the variable Neoproterozoic deposit compositions.
3) We favor that the Bikou terrane connected with the Yangtze Block under convergent settings during the early-middle Neoproterozoic. Subsequently, this region was most likely under extensional settings after the termination of subduction, arc magmatism and orogenic processes.

CRediT authorship contribution statement

Zhidong Gu: Investigation, Methodology, Validation, Visualization, Formal analysis, Writing – original draft, Writing – review & editing, Funding acquisition. **Xing Jian:** Investigation, Methodology, Validation, Visualization, Formal analysis, Writing – original draft, Writing – review & editing, Funding acquisition. **Guixia Liu:** Investigation, Resources, Visualization, Formal analysis. **Xiaotian Shen:** Investigation, Visualization, Formal analysis, Data curation. **Hanjing Fu:** Investigation, Visualization, Formal analysis, Data curation. **Xiufen Zhai:** Investigation, Resources. **Hua Jiang:** Investigation, Resources.

Declaration of Competing Interest

The authors declare that they have no known competing financial interests or personal relationships that could have appeared to influence the work reported in this paper.

Data availability

Data will be made available on request.

Acknowledgements

We would like to thank Peizhi Wang, Zemin Bao, and Shoujie Liu for their assiatance in the SHRIMP analyses. We are grateful to Ruizhi Liuzhu for his fieldwork during 2020-2021 and Xiaolei Wang and Junyong Li for their fieldwork during 2014-2015. Ling Wang, Xiaoli Dong and Shuhuai Ye from Xiamen University contributed to some lab analysis and graphing in this study. We also appreciate the editor and two reviewers very much for their constructive comments and suggestions. This project was supported from the Science and Technology Project of PetroChina (2021DJ0501, 2022KT0101, and KT2020-01-03) and the National Petroleum Project of China (no. 2016ZX05004005-001).

Appendix A. Supplementary data

Supplementary data to this article can be found online at https://doi.org/10.1016/j.precamres.2023.107197.

References

Ai, J., Zhong, N., George, S.C., Zhang, Y., Yao, L., Wang, T., 2020. Evolution of paleo-weathering during the late Neoproterozoic in South China: Implications for paleoclimatic conditions and organic carbon burial. Palaeogeogr. Palaeoclimatol. Palaeoecol. 555, 109843.
Bao, X., Zhang, S., Jiang, G., Wu, H., Li, H., Wang, X., An, Z., Yang, T., 2018. Cyclostratigraphic constraints on the duration of the Datangpo Formation and the onset age of the Nantuo (Marinoan) glaciation in South China. Earth Planet. Sci. Lett. 483, 52–63.
Bhatia, M.R., Crook, K.A., 1986. Trace element characteristics of graywackes and tectonic setting discrimination of sedimentary basins. Contrib. Miner. Petrol. 92 (2), 181–193.
Cawood, P.A., Hawkesworth, C.J., Dhuime, B., 2012. Detrital zircon record and tectonic setting. Geology 40 (10), 875–878.
Cawood, P.A., Wang, Y., Xu, Y., Zhao, G., 2013. Locating South China in Rodinia and Gondwana: A fragment of greater India lithosphere? Geology 41 (8), 903–906.
Chen, X., Kuang, H., Liu, Y., Le Heron, D.P., Wang, Y., Peng, N., Wang, Z., Zhong, Q., Yu, H., Chen, J., 2021. Revisiting the Nantuo Formation in Shennongjia, South China: A new depositional model and multiple glacial cycles in the Cryogenian. Precambr. Res. 356, 106132.
Condon, D.J., Prave, A.R., Benn, D.I., 2002. Neoproterozoic glacial-rainout intervals: observations and implications. Geology 30 (1), 35–38.
Cui, X., Zhu, W.B., Ge, R.F., 2014. Provenance and crustal evolution of the northern Yangtze Block revealed by detrital zircons from Neoproterozoic-Early Paleozoic sedimentary rocks in the Yangtze Gorges area, South China. J. Geol. 122 (2), 217–235.
Dalziel, I.W., 1997. OVERVIEW: Neoproterozoic-Paleozoic geography and tectonics: Review, hypothesis, environmental speculation. Geol. Soc. Am. Bull. 109 (1), 16–42.
Deru, X., Xuexiang, G., Pengchun, L., Guanghao, C., Bin, X., Bachlinski, R., Zhuanli, H., Gonggu, F., 2007. Mesoproterozoic-Neoproterozoic transition: Geochemistry, provenance and tectonic setting of clastic sedimentary rocks on the SE margin of the Yangtze Block, South China. J. Asian Earth Sci. 29 (5–6), 637–650.
Dickinson, W.R., 1985. Interpreting provenance relations from detrital modes of sandstones. Provenance of Arenites 333–361.
Ding, Z., Yao, S., Zhou, Z., Fang, J., 1998. Tectonic attribute of the mid-Proterozoic Bikou terrane. Geotecton. Metallog. 22 (3), 219–226. In Chinese with English abstract.
Domeier, M., 2018. Early Paleozoic tectonics of Asia: Towards a full-plate model. Geosci. Front. 9 (3), 789–862.
Dong, Y., Santosh, M., 2016. Tectonic architecture and multiple orogeny of the Qinling Orogenic Belt, Central China. Gondwana Research 29 (1), 1–40.
Dong, Y., Zhang, X., Liu, X., Li, W., Chen, Q., Zhang, G., Zhang, H., Yang, Z., Sun, S., Zhang, F., 2015. Propagation tectonics and multiple accretionary processes of the Qinling Orogen. J. Asian Earth Sci. 104, 84–98.
Druschke, P., Hanson, A.D., Yan, Q., Wang, Z., Wang, T., 2006. Stratigraphic and U-Pb SHRIMP detrital zircon evidence for a Neoproterozoic continental arc, central China: Rodinia implications. J. Geol. 114 (5), 627–636.
Du, Q., Wang, Z., Wang, J., Qiu, Y., Jiang, X., Deng, Q., Yang, F., 2013. Geochronology and paleoenvironment of the pre-Sturtian glacial strata: Evidence from the Liantuo Formation in the Nanhua rift basin of the Yangtze Block, South China. Precambr. Res. 233, 118–131.
Fedo, C.M., Wayne Nesbitt, H., Young, G.M., 1995. Unraveling the effects of potassium metasomatism in sedimentary rocks and paleosols, with implications for paleoweathering conditions and provenance. Geology 23 (10), 921–924.
Floyd, P.A., Leveridge, B.E., 1987. Tectonic environment of the Devonian Gramscatho basin, south Cornwall: framework mode and geochemical evidence from turbiditic sandstones. J. Geol. Soc. London 144 (4), 531–542.
Fu, H., Jian, X., Liang, H., Zhang, W., Shen, X., Wang, L., 2022. Tectonic and climatic forcing of chemical weathering intensity in the northeastern Tibetan Plateau since the middle Miocene. Catena 208, 105785.
Gao, F., Pei, X., Li, R., Li, Z., Pei, L., Chen, Y., Wang, M., Zhao, S., Liu, C., Li, X., 2020a. Further constraints on a Neoproterozoic active continental margin from sandstones of the Hengdan Group in the Bikou Terrane, northwestern margin of the Yangtze Block, South China. J. Asian Earth Sci. 203, 104514.
Gao, F., Pei, X., Li, R., Li, Z., Pei, L., Chen, Y., Wang, M., Zhao, S., Liu, C., Li, X., 2020b. Neoproterozoic tectonic evolution of the northwestern margin of the Yangtze Block (southwestern China): Evidence from sandstone geochemistry and detrital zircon U-Pb ages of the Hengdan Group. Precambr. Res. 344, 105737.
Gu, Z., Jian, X., Watts, A.B., Zhai, X., Liu, G., Jiang, H., 2023. Formation and evolution of an Early Cambrian foreland basin in the northwest Yangtze Block, South China. J. Geol. Soc. London 180 (3).

Heinrich, H., 1988. Origin and consequences of cyclic ice rafting in the northeast Atlantic Ocean during the past 130,000 years. Quat. Res. 29 (2), 142–152.
Hoffman, P.F., Kaufman, A.J., Halverson, G.P., Schrag, D.P., 1998. A Neoproterozoic snowball earth. Science 281 (5381), 1342–1346.
Huang, K.J., Teng, F.Z., Shen, B., Xiao, S., Lang, X., Ma, H.R., Fu, Y., Peng, Y., 2016. Episode of intense chemical weathering during the termination of the 635 Ma Marinoan glaciation. Proceedings of the National Academy of Sciences 113(52), 14904–14909.
Hubert, J.F., 1962. A zircon-tourmaline-rutile maturity index and the interdependance of the composition of heavy mineral assemblages with the gross composition and texture of sandstones. J. Sediment. Petrol. 32, 440–450.
Hui, B., Dong, Y., Cheng, C., Long, X., Liu, X., Yang, Z., Sun, S., Zhang, F., Varga, J., 2017. Zircon U-Pb chronology, Hf isotope analysis and whole-rock geochemistry for the Neoarchean-Paleoproterozoic Yudongzi complex, northwestern margin of the Yangtze craton, China. Precambr. Res. 301, 65–85.
Hui, B., Dong, Y., Zhang, F., Sun, S., Liu, X., Cheng, C., He, D., 2019. Geochronology and geochemistry of ca. 2.48 Ga granitoid gneisses from the Yudongzi Complex in the north-western Yangtze Block, China. Geological Journal 54 (2), 879–896.
Hui, B., Dong, Y., Liu, G., Zhao, H., Sun, S., Zhang, F., Liu, X., 2020. Origin of mafic intrusions in the Micangshan Massif, Central China: Implications for the Neoproterozoic tectonic evolution of the northwestern Yangtze Block. J. Asian Earth Sci. 190, 104132.
Hui, B., Dong, Y., Zhang, F., Sun, S., He, S., 2021. Neoproterozoic active margin in the northwestern Yangtze Block, South China: new clues from detrital zircon U-Pb geochronology and geochemistry of sedimentary rocks from the Hengdan Group. Geol. Mag. 158 (5), 842–858.
Jian, X., Guan, P., Zhang, W., Feng, F., 2013. Geochemistry of Mesozoic and Cenozoic sediments in the northern Qaidam basin, northeastern Tibetan Plateau: implications for provenance and weathering. Chem. Geol. 360, 74–88.
Jian, X., Weislogel, A., Pullen, A., 2019a. Triassic sedimentary filling and closure of the eastern paleo-Tethys Ocean: New insights from detrital zircon geochronology of Songpan-Ganzi, Yidun, and west Qinling flysch in eastern Tibet. Tectonics 38 (2), 767–787.
Jian, X., Zhang, W., Liang, H., Guan, P., Fu, L., 2019b. Mineralogy, petrography and geochemistry of an early Eocene weathering profile on basement granodiorite of Qaidam basin, northern Tibet: Tectonic and paleoclimatic implications. Catena 172, 54–64.
Jian, X., Weislogel, A., Pullen, A., Shang, F., 2020a. Formation and evolution of the Eastern Kunlun Range, northern Tibet: Evidence from detrital zircon U-Pb geochronology and Hf isotopes. Gondw. Res. 83, 63–79.
Jian, X., Yang, S., Hong, D., Liang, H., Zhang, S., Fu, H., Zhang, W., 2020b. Seasonal geochemical heterogeneity of sediments from a subtropical mountainous river in SE China. Mar. Geol. 422, 106120.
Jian, X., Fu, L., Wang, P., Guan, P., Zhang, W., Fu, H., Mei, H., 2023. Sediment provenance of the Lulehe Formation in the Qaidam basin: Insight to initial Cenozoic deposition and deformation in northern Tibetan Plateau. Basin Res. 35, 271–294.
Jiang, G., Shi, X., Zhang, S., Wang, Y., Xiao, S., 2011. Stratigraphy and paleogeography of the Ediacaran Doushantuo Formation (ca. 635–551 Ma) in south China. Gondw. Res. 19 (4), 831–849.
Kuang, Y., Zhang, B., Ouyang, J., 1999. Decomposition and stratigraphic subdivision of Bikou Group in northeastern margin of Yangtze Craton. J. China Univ. Geosci.: Earth Sci. 24 (3), 251–255. In Chinese with English abstract.
Lai, S., Li, Y., Qin, J., 2007. Geochemistry and LA-ICP-MS zircon U-Pb dating of the Dongjiahe ophiolite complex from the western Bikou terrane. Sci. China Ser. D Earth Sci. 50, 305–313.
Lan, Z., Li, X.H., Zhu, M., Zhang, Q., Li, Q.L., 2015. Revisiting the Liantuo Formation in Yangtze Block, South China: SIMS U-Pb zircon age constraints and regional and global significance. Precambr. Res. 263, 123–141.
Lang, X., Chen, J., Cui, H., Man, L., Huang, K.J., Fu, Y., Zhou, C., Shen, B., 2018. Cyclic cold climate during the Nantuo glaciation: evidence from the Cryogenian Nantuo Formation in the Yangtze Block, South China. Precambr. Res. 310, 243–255.
Le Heron, D.P., Tofaif, S., Vandyk, T., Ali, D.O., 2017. A diamictite dichotomy: Glacial conveyor belts and olistostromes in the Neoproterozoic of Death Valley, California, USA. Geology 45 (1), 31–34.
Lenton, T.M., Boyle, R.A., Poulton, S.W., Shields-Zhou, G.A., Butterfield, N.J., 2014. Co-evolution of eukaryotes and ocean oxygenation in the Neoproterozoic era. Nat. Geosci. 7 (4), 257–265.
Li, K., Deng, Q., Wang, J., Hou, M., Yakymchuk, C., Cui, X., Ren, G., Wang, Z., Dai, J., Chen, B., 2020. Detrital zircon in the Huashan Group, northern Yangtze Block: Implications for the nature of Neoproterozoic sedimentary basins and Precambrian crustal evolution. Geol. J. 55 (12), 8211–8224.
Li, Y., Lai, S., Qin, J., 2006. Further study on geochemical characteristics and genesis of the boninitic rocks from bikou group, Northern Yangtze plate. J. China Univ. Geosci. 17 (2), 126–131.
Li, Y., Lai, S., Qin, J., Liu, X., Wang, J., 2007. Geochemical characteristics of Bikou volcanic group and Sr-Nd-Pb isotopic composition: Evidence for breakup event in the north margin of Yangtze plate, Jining era. Sci. China Ser. D Earth Sci. 50 (Suppl. 2), 339–350.
Li, J.Y., Wang, X.L., Gu, Z.D., 2018. Early Neoproterozoic arc magmatism of the Tongmuliang Group on the northwestern margin of the Yangtze Block: implications for Rodinia assembly. Precambr. Res. 309, 181–197.
Liu, X., Gao, S., Diwu, C., Ling, W., 2008. Precambrian crustal growth of Yangtze Craton as revealed by detrital zircon studies. Am. J. Sci. 308 (4), 421–468.
Lu, H., Wang, Z., Wang, T., Jiang, C., 2005. Sedimentary environment and provenance of the Guanjiagou Formation of the western Qinling Mountains. Geoscience 19 (3), 394–402. In Chinese with English abstract.
Lu, H., Wang, Z., Wang, T., Jiang, C., 2006. Provenance analysis of the Guanjiagou Formation in West Qinling. Acta Geol. Sin. 80 (4), 508–516. In Chinese with English abstract.
Mao, F., Pei, X., Li, R., Li, Z., Pei, L., Liu, C., Zhao, S., Gao, F., Chen, Y., Zhou, H., 2021. The LA-ICP-MS U-Pb dating of detrital zircons from the Nanhua System in Bikou Terrane, northwestern margin of Yangtze Block. Sediment. Geol. Tethyan Geol. 41 (1), 41–57. In Chinese with English abstract.
McDonough, W.F., Sun, S.S., 1995. The composition of the Earth. Chem. Geol. 120 (3–4), 223–253.
McLennan, S.M., Hemming, S., McDaniel, D.K., Hanson, G.N., 1993. Geochemical approaches to sedimentation, provenance, and tectonics. Special Papers-Geological Society of America 21–40.
Mei, H., Jian, X., Zhang, W., Fu, H., Zhang, S., 2021. Behavioral differences between weathering and pedogenesis in a subtropical humid granitic terrain: Implications for chemical weathering intensity evaluation. Catena 203, 105368.
Meng, Q.R., Zhang, G.W., 1999. Timing of collision of the North and South China blocks: controversy and reconciliation. Geology 27 (2), 123–126.
Meng, Q.R., Zhang, G.W., 2000. Geologic framework and tectonic evolution of the Qinling orogen, central China. Tectonophysics 323 (3–4), 183–196.
Merdith, A.S., Collins, A.S., Williams, S.E., Pisarevsky, S., Foden, J.D., Archibald, D.B., Blades, M.L., Alessio, B.L., Armistead, S., Plavsa, D., Clark, C., Müller, R.D., 2017. A full-plate global reconstruction of the Neoproterozoic. Gondw. Res. 50, 84–134.
Och, L.M., Shields-Zhou, G.A., 2012. The Neoproterozoic oxygenation event: Environmental perturbations and biogeochemical cycling. Earth Sci. Rev. 110 (1–4), 26–57.
Pei, X., 1989. The features and the tectonic significance of rock assemblage in the Bikou Group, southern Qinling. J. Xi'an College Geol. 11 (2), 46–56. In Chinese with English abstract.
Pei, X., Ding, S., Hu, B., Li, Y., Zhang, G., Guo, J., 2004. Definition of the Guanzizhen ophiolite in Tianshui area, western Qinling, and its geological significance. Geol. Bull. Chin 23 (12), 1202–1208. In Chinese with English abstract.
Pi, D.H., Jiang, S.Y., 2016. U-Pb dating of zircons from tuff layer, sandstone and tillite samples in the uppermost Liantuo Formation and the lowermost Nantuo Formation in Three Gorges area, South China. Geochemistry 76 (1), 103–109.
Qi, L., Cawood, P.A., Yang, J., Xu, Y., Du, Y., 2020. Quantifying temperature variation between Neoproterozoic cryochron-nonglacial interlude, Nanhua Basin, South China. Precambrian Research 351, 105967.
Qin, K., Jin, H., Zhao, D., 1994. Tectonic evolution and mineralization in Bikou ancient island arc belt. Henan Geology 12 (4), 304–317. In Chinese with English abstract.
Rodríguez-López, J.P., Liesa, C.L., Pardo, G., Meléndez, N., Soria, A.R., Skilling, I., 2016. Glacial dropstones in the western Tethys during the late Aptian–early Albian cold snap: Palaeoclimate and palaeogeographic implications for the mid-Cretaceous. Palaeogeogr. Palaeoclimatol. Palaeoecol. 452, 11–27.
Rudnick, R.L., Gao, S., 2014. The crust. Treatise on Geochemistry; Kelemen, P., Hanghøj, K., Greene, A., Eds.
Su, C., Liu, J., Wang, Y., 2003. Submarine fan depositional systems of the Guanjiagou Formation in Wenxian, West Qinling. J. Chang'an University (Earth Science Edition) 25 (4), 21–26. In Chinese with English abstract.
Sun, W.H., Zhou, M.F., Yan, D.P., Li, J.W., Ma, Y.X., 2008. Provenance and tectonic setting of the Neoproterozoic Yanbian Group, western Yangtze block (SW China). Precambr. Res. 167 (1–2), 213–236.
Sun, W.H., Zhou, M.F., Gao, J.F., Yang, Y.H., Zhao, X.F., Zhao, J.H., 2009. Detrital zircon U-Pb geochronological and Lu–Hf isotopic constraints on the Precambrian magmatic and crustal evolution of the western Yangtze Block, SW China. Precambrian Research 172 (1–2), 99–126.
Vermeesch, P., 2012. On the visualisation of detrital age distributions. Chem. Geol. 312, 190–194.
Walker, J.D., and Geissman, J.W., compilers, 2022. Geologic Time Scale v. 6.0: Geological Society of America, https://doi.org/10.1130/2022.CTS006C.
Wang, W., Cawood, P.A., Pandit, M.K., Xia, X., Raveggi, M., Zhao, J., Zheng, J., Qi, L., 2021. Fragmentation of South China from greater India during the Rodinia-Gondwana transition. Geology 49 (2), 228–232.
Wang, L.J., Griffin, W.L., Yu, J.H., O'Reilly, S.Y., 2010a. Precambrian crustal evolution of the Yangtze Block tracked by detrital zircons from Neoproterozoic sedimentary rocks. Precambr. Res. 177 (1–2), 131–144.
Wang, L.J., Griffin, W.L., Yu, J.H., O'Reilly, S.Y., 2013. U-Pb and Lu–Hf isotopes in detrital zircon from Neoproterozoic sedimentary rocks in the northern Yangtze Block: implications for Precambrian crustal evolution. Gondw. Res. 23 (4), 1261–1272.
Wang, J., Li, X., Duan, T., Liu, D., Song, B., Li, Z., Gao, Y., 2003. Zircon SHRIMP U-Pb dating for the Cangshuipu volcanic rocks and its implications for the lower boundary age of the Nanhua strata in South China. Chin. Sci. Bull. 48, 1663–1669.
Wang, X.C., Li, X.H., Li, W.X., Li, Z.X., Liu, Y., Yang, Y.H., Liang, X.R., Tu, X.L., 2008. The Bikou basalts in the northwestern Yangtze block, South China: Remnants of 820–810 Ma continental flood basalts? Geol. Soc. Am. Bull. 120 (11–12), 1478–1492.
Wang, Y., Wang, Y., Su, C., 2010b. Discovery and its geological significance of micropalaeoflora from Guanjiagou Group in Wenxian county, Gansu Province. J. Earth Sci. Environ. 32 (1), 40–43. In Chinese with English abstract.
Wang, R., Xu, Z., Santosh, M., 2023. Mid– late Neoproterozoic tectonic evolution of the northern margin of the Yangtze Block, South China, as constrained from the detrital zircon record. GSA Bull. 135 (5–6), 1449–1466.
Wang, Z., Yin, C., Gao, L., Tang, F., Liu, Y., Liu, P., 2006. The Character of the Chemical Index of Alteration and discussion of subdivision and correlation of the Nanhua System in Yichang area. Geol. Rev. 52 (5), 577–585. In Chinese with English abstract.

Wang, L.J., Yu, J.H., Griffin, W.L., O'Reilly, S.Y., 2012. Early crustal evolution in the western Yangtze Block: evidence from U-Pb and Lu–Hf isotopes on detrital zircons from sedimentary rocks. Precambr. Res. 222, 368–385.
Wang, W., Zhou, M.F., 2012. Sedimentary records of the Yangtze Block (South China) and their correlation with equivalent Neoproterozoic sequences on adjacent continents. Sed. Geol. 265, 126–142.
Wang, W., Zhou, M.F., 2013. Petrological and geochemical constraints on provenance, paleoweathering, and tectonic setting of the Neoproterozoic sedimentary basin in the eastern Jiangnan Orogen, South China. J. Sediment. Res. 83 (11), 975–994.
Wu, T., Wang, X.C., Li, W.X., Wilde, S.A., Tian, L., 2019. Petrogenesis of the ca. 820–810 Ma felsic volcanic rocks in the Bikou Group: Implications for the tectonic setting of the western margin of the Yangtze Block. Precambr. Res. 331, 105370.
Xia, Z., Xia, L., Xu, X., Zhao, J., 1999. The nature and formation environment of Volcanic rock series of the Bikou Group. Geol. Rev. 45 (S1), 681–688. In Chinese with English abstract.
Xiao, L., Zhang, H.F., Ni, P.Z., Xiang, H., Liu, X.M., 2007. LA-ICP-MS U-Pb zircon geochronology of early Neoproterozoic mafic-intermediat intrusions from NW margin of the Yangtze Block, South China: Implication for tectonic evolution. Precambr. Res. 154 (3–4), 221–235.
Xu, X., Xia, Z., Xia, L., 2002. Volcanic cycles of the Bikou Group and their tectonic implications. Geol. Bull. China 21 (8), 478–485. In Chinese with English abstract.
Yan, Q.R., Wang, Z., Yan, Z., Hanson, A.D., Druschke, P.A., Liu, D., Song, B., Jian, P., Wang, T., 2003. The ages of the Bikou Group volcanic rocks: SHRIMP zircon U-Pb dating results. Geol. Bull. China 22 (6), 456–458. In Chinese with English abstract.
Yan, Q.R., Hanson, A.D., Wang, Z., Druschke, P.A., Yan, Z., Wang, T., Lu, H., 2004a. Timing and setting of Guanjiagou conglomerate in South Qinling and their tectonic implications. Chin. Sci. Bull. 49 (16), 1722–1729.
Yan, Q.R., Hanson, A.D., Wang, Z., Druschke, P.A., Yan, Z., Wang, T., Liu, D., Song, B., Jian, P., Zhou, H., Jiang, C., 2004b. Neoproterozoic subduction and rifting on the northern margin of the Yangtze Plate, China: implications for Rodinia reconstruction. Int. Geol. Rev. 46 (9), 817–832.
Yan, D.P., Zhou, Y., Qiu, L., Wells, M.L., Mu, H., Xu, C.G., 2018. The Longmenshan tectonic complex and adjacent tectonic units in the eastern margin of the Tibetan Plateau: a review. J. Asian Earth Sci. 164, 33–57.
Yang, F., Zhou, X., Hu, Y., Yang, X., Yang, R., 2022. Neoproterozoic extensional basins and its control on the distribution of hydrocarbon source rocks in the Yangtze Craton, South China. Geosystems and Geoenvironment 1 (1), 100015.
Yin, C., Liu, D., Gao, L., Wang, Z., Xing, Y., Jian, P., Shi, Y., 2003. Lower boundary age of the Nanhua System and the Gucheng glacial stage: evidence from SHRIMP II dating. Chin. Sci. Bull. 48, 1657–1662. In Chinese with English abstract.
Yu, J.H., O'Reilly, S.Y., Wang, L., Griffin, W.L., Zhang, M., Wang, R., Jiang, S., Shu, L., 2008. Where was South China in the Rodinia supercontinent?: evidence from U-Pb geochronology and Hf isotopes of detrital zircons. Precambr. Res. 164 (1–2), 1–15.
Zhang, G.W., Meng, Q.G., Yu, Z.P., Sun, Y., Zhou, D.W., Guo, A.L., 1996. Orogenesis and dynamics of the Qinling orogen. Sci. China. Ser. D Earth Sci. 39 (3), 225–234.
Zhao, G., Cawood, P.A., 2012. Precambrian geology of China. Precambr. Res. 222, 13–54.
Zhao, M.Y., Zheng, Y.F., 2015. The intensity of chemical weathering: Geochemical constraints from marine detrital sediments of Triassic age in South China. Chem. Geol. 391, 111–122.